(4)

SECOND SEMIANNUAL REPORT

for period

15 July 1990 through 14 January 1991

AUTOMATED HANDLING AND ASSEMBLING OF NON-~~RIDGE~~ OBJECTS

RIDGED

for

OFFICE OF NAVAL RESEARCH

on

Contract No. N-00014-90-J-1516

by

Yuan F. Zheng, Principal Investigator
Dept. of Electrical Engineering
The Ohio State University
Columbus, OH 43210

TABLE OF CONTENTS

1. INTRODUCTION

This is the second semiannual report on the research project entitled "Automated Handling and Assembling of Non-rigid Objects", covering the period July 15, 1990 through January 14, 1991. In this period, three topics were studied. The first topic addresses the strategies of automated handling and assembling of non-rigid objects by using multiple end-effectors, the second topic studies the shape reconstruction of two dimensional objects, and the third topic is the construction of a laser range finder for identification of the third dimension of an object.

The purpose of the first topic is to investigate optimal tool structures for handling one and two dimensional objects. Previously, we proposed to use vacuum pads to pick up large deformable sheet by the difference of the air pressure. Such a mechanism needs a large pad when the object has a large surface area, which is often too heavy for numerically controlled machine to carry. By using two ordinary end-effectors, just like the two hands of human beings, deformable objects can be manipulated without using a large tool. Our study has developed an optimal mechanism for coordinating the end-effectors such that the machine consumes the minimum energy and no damage is made to the object.

The purpose of the second topic is to identify the deformed shape of two-dimensional objects. For two dimensional objects, there does not exist closed-form solution to the governing equation of the deformation. Our goal is to sense a few data points on the deformed surface. Based on these points, a numerical model can be driven which can reconstruct the entire surface with a good approximation. This numerical model can also be modified in accordance with the deformation behavior of the object.

The purpose of the third topic is to develop a laser range finder such that all three dimensions of an object can be identified. The laser range finder is a very important tool for our research, since a two-dimensional object becomes three dimensional once it is deformed. For three dimensional objects, the third dimension is important to completely identify the shape of an object even before the deformation occurs.

The rest of this report describes the results or the status of the three topics as just summarized as well as the research plan for the next period.

2. AUTOMATED HANDLING OF DEFORMABLE OBJECTS BY COORDINATED MANIPULATORS

Traditionally, large two-dimensional objects are handled by vacuum pads. The pads are designed to cover the most area of the object surface. When the space inside the pad becomes vacuum, the material can be picked up by the difference of the air pressure. A vacuum pad, however, may become very heavy and big when the object surface is large. This imposes a large load on the machines on which the pad is installed. Human beings, on the other hand, can effectively handle large deformable objects with two hands. This implies that by coordinating two manipulators, the same object may be handled by ordinary end-effectors. The mechanism for handling deformable objects, however, is very different from handling rigid objects. A major difference is that the two end-effectors have certain degrees of freedom in their relative motions. This motion freedom can be used to satisfy other requirements in the automated handling of the objects. For example, reducing the distance between the two end-effectors can reduce the workspace required by the automation process. The question is what are the optimal motion trajectories for each end-effector in handling the objects?

We study this problem by using two criterion. First, the load imposed to the handling machine should be as small as possible, and second, the possibility of damage to the object should also be as small as possible. Since the flexibility of the object, the relative position and orientation of the two end-effectors can be altered while handling the object. When the object is deformed, however, deformation forces and moments are exerted on the end-effectors and the objects. Large deformation forces and moments may damage the object and impose a large load on the handling machine.

Three coordinating methods are suggested for the two manipulators. The first method allows the relative orientation between the end-effectors to be altered, but no relative position changes. The second method allows the relative position to be altered, but no relative orientation changes. The third method allows both the position and orientation to be changed. Through the analysis of kinematic constraints, the first method is found not possible. Studies are then concentrated on the second and third methods. The second and third methods are

further compared through the study of deformation mechanics. It is shown that the third method results in minimum reaction forces and moments between the objects and end-effectors. It is identified as the best method for automated handling of two dimensional and deformable objects.

Unfortunately, motion trajectories for the two manipulators to handle the object are very complicated to compute, which is not adequate for real-time execution. For practical applications, we further propose a simplified method in which the complicated trajectories are replaced by piece-wise linear functions. The reaction forces and moments in the simplified method are also analyzed which are only slightly larger than the original method.

To verify the proposed method, experiments are also conducted in our Advanced Manufacturing Laboratory . The experiment results show that the third method (Fig. 1) is better than the second method. By using the second method, the orientation of the two end-effectors are kept unchanged while they approach each other in order to bend the object. This exerts large reaction forces and moments on the objects, leaving two permanent crease on the object surface. By using the third method, the end-effector simultaneously alter their position and orientation while bending the object, and no permanent damage is made on the object. In addition, the forces and moments exerted on the end-effectors are much smaller than that in the second method.

A technical paper has been written based on the research results just described, which is attached as Appendix A of this report. Technical details of the handling mechanism by two manipulators can be found in the paper.

3. SHAPE RECONSTRUCTION OF TWO DIMENSIONAL OBJECTS

Shape reconstruction of two-dimensional objects is a special problem associated with the automated handling and assembling of deformable objects. When a two-dimensional object is picked up by an end-effector, the object is deformed. In order to precisely position it, the deformed shape needs to be identified. There are two difficulties associated with this identification task. First, the deformation characteristics of the object are unknown; therefore, it is impossible to reconstruct the surface by using its deformation governing equations.

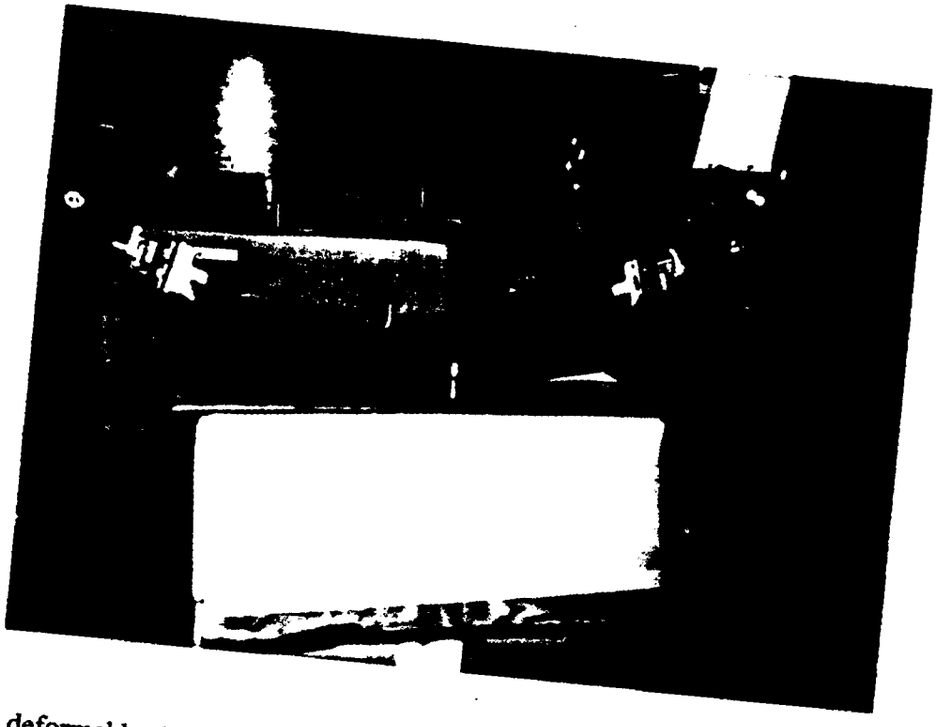

Fig. 1 A deformable sheet is handled by two manipulators using the third method. Note that both the position and orientation of the two end-effectors are altered as the object is picked up.

Secondly, even the governing equation is identified (like what we have done for one-dimensional objects), there is no explicit and closed-form solution to the governing equation of two-dimensional objects.

We propose to use numerical solutions to represent the deformed surface. To precisely represent the surface of the object, it appears that a great number of data need to be collected from the object surface. This imposes a heavy load on the sensing system, and makes the methods inefficient. To overcome this problem, we propose a physically-based method. Two steps are involved in the method. The first step is to determine how to describe a deformed object by using only sparse data on the object surface. The second step is to decide sensing strategies, i.e., how to select the points on the surface that need to be sensed.

The principle of physically-based modeling for vision can be stated as follows: physical properties and/or high level knowledge of the objects should be considered in both their representation and the low level sensing tasks of the vision sensor. Thus the shape can be reconstructed by using sparse data points of the surface as the rest of the surface should be governed by the physical properties of the object. If this principle is applied to shape reconstruction of a two-dimensional object, the deformation governing equations of the plate should be used to derive the representation of the objects. However, as mentioned earlier, this is not possible. Instead of strictly following the deformation governing equations, we propose a **physical constraint** concept, i.e., physical constraints associated with a deformable object should be considered when the shape is constructed. The physical constraints include the elastic deformation of two-dimensional object, the shape of the object before deformation, and the position and orientation of the gripper that holds the object. These constraints are already known and should be taken into consideration in the process of reconstruction.

In order to reflect the elastic nature of the object, the shape of the object is proposed to be reconstructed by minimizing the strain energy of the object surface. As the expression of the plate's strain energy is very complex, it is simplified for the purpose of efficient computation. This simplified strain energy happens to be the same as the energy functional of the **thin plate spline** (TPS) used in visual surface reconstruction. A pioneering work in visual surface reconstruction is accomplished by Grimson [1]. Terzopoulos [2] gave a more rigorous proof of the TPS in reconstructing the surface from given sparse data point. Both Grimson and Terzopoulos used energy minimization methods to reconstruct the surface. Their method is adopted in our reconstruction process.

In the work of visual reconstruction done by Grimson and Terzopoulos, the sparse set of data points is provided by stereo visions. We propose to use a laser range finder in our shape reconstruction process. The advantage of using the range finder is that we can control the sensor to sense the data points we want. The range finder can be moved by a robot arm. Hence, the sensor is dynamic. We thus have to decide sensing strategies for the range finder.

The basic strategy is that we need to sense dense data points from the region where the the surface curvatures are large and sparse data points from the area where the surface curvatures

are small. The physical constraints as mentioned earlier can determine whether the curvatures on a particular part of the surface are large or small.

At the point of this writing, this reconstruction topic is still under active investigation. We expect that a detailed technical report will be available when we submit next semiannual report.

4. THE CONSTRUCTION OF A LASER RANGE FINDER

In order to carry on experimental study in our research, a laser range finder was constructed in this research period. The basic structure of the laser range finder is as shown in Fig. 2. It consists of a laser and a CCD camera. The laser generates a beam light source which is converted into a sheet of light through a cylindrical lens. This sheet of light is scanned across the scene, producing a single light stripe for each position. When the light stripe is sensed by the CCD camera, the camera view of the stripe shows displacements along a stripe which are proportional to depth. Thus, a structured light source plus a two-dimensional sensor can provide three-dimensional information. Three-dimensional information is essential for us to study the deformation behavior of two and three-dimensional objects.

At the point of this writing, the laser range finder is already operational. Appendix B of this report describes how to locate a point and a surface in a three-dimensional space knowing only information about their image captured by the range finder.

5. RESEARCH PLAN FOR THE NEXT SEMIANNUAL PERIOD

In the next period, we plan to continue our research on the reconstruction of the two-dimensional object as described in the third section of this report. In addition, we will start to look at the virtual space issue as mentioned in our proposal. This issue is for planning the motion control mechanism of the host machines which handle the object. The basic idea is to use a virtual space to enclose the shape of a deformable object. As a result, the deformed shape of an object does not need to be exactly identified as long as it falls in the virtual space. In this

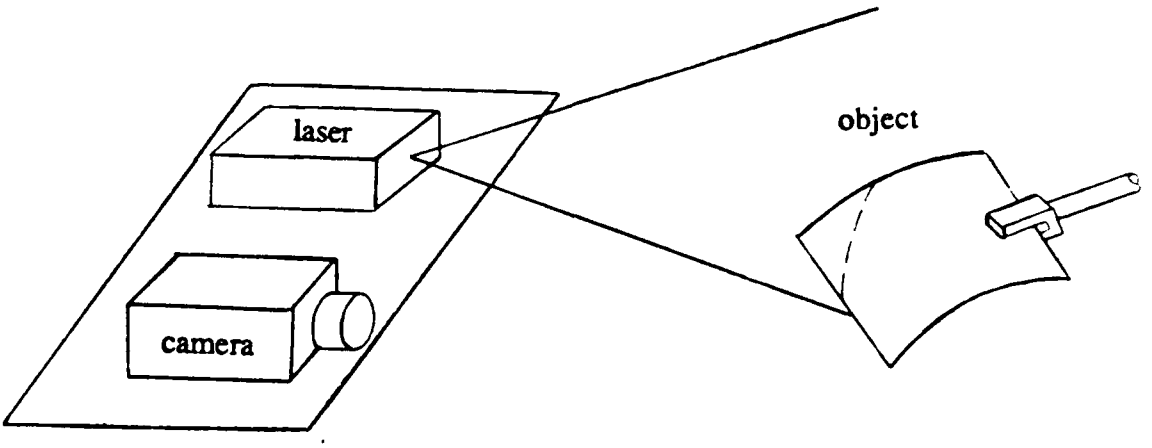

Fig. 2 The structure of the range finder

way, we can plan the motion trajectory of the host machine based on the virtual space, and can still avoid collisions of the object with any other obstacles.

Another topic that we will initiate is the deformation of three-dimensional objects. We will first study how a three-dimensional object is deformed under external forces and moments. Then, we will investigate how to recognize a three-dimensional object when it is deformed.

REFERENCES

1. W.E. Grimson, From Image to Surface: A Computational Study of the Human Early Visual System, MIT Press, Cambridge, MA, 1981.

2. D. Terzopoulos, "Multilevel Reconstruction of Visual Surface: Variational Principles and Finite-Element Representation," in Multiresolution Image Processing and Analysis, Spring-Verlag, New York, 1984.

APPENDIX A

AUTOMATED HANDLING OF DEFORMABLE OBJECTS BY COORDINATED MANIPULATORS

Ming Z. Chen and Yuan F. Zheng
Department of Electrical Engineering
The Ohio State University
Columbus, OH 43210

ABSTRACT

Coordinating two manipulators to automatically handle deformable objects is studied in this paper. Because of the flexibility of the objects, the manipulator hands are allowed to have certain degrees of freedom in their relative motions. However, kinematic constraints are still imposed on the relative motions between the two manipulators. In this study, the kinematic constraints are first derived from the flexibility of the objects. Then the investigation is concentrated on the mechanisms for handling one-dimensional objects. Three coordinating methods are identified for the manipulators. The first method allows the relative orientation between the two manipulator end-effectors to be altered, but no relative position changes. The second method allows the relative position to be altered, but no relative orientation changes. The third method allows both the position and the orientation to be altered. Through the analysis of the object mechanics, it is found that the first method is not adequate. Motion trajectories of the end-effectors are then derived for the second and third methods. Analysis also shows that the third method results in the minimum reaction forces and moments between the object and the hands. It is best to use for automated handling of one or two dimensional deformable objects. Finally, experimental results are presented to verify the theoretical studies.

ACKNOWLEDGEMENT: This work is supported by ONR under grant N00014-90-J-1516, and by a Presidential Young Investigator Award of NSF to Yuan F. Zheng (DDM-8996238).

1. INTRODUCTION

In recent years, coordinating two or more robot manipulators for manufacturing automation has received much research attention. An earlier investigation was conducted by Konstantinov and Markov [1]. In their work, some necessary conditions for the collaboration of two end-effectors in assembly operations were given. Later, multiple manipulators working in a common workspace were studied by Freund [2]. His main interest was to avoid collisions among multiple manipulators, for which a hierarchical control system was developed, and a nonlinear control mechanism was used in the system.

Theoretical studies of kinematic constraints imposed on two coordinating robots handling a rigid object were conducted by Mason [3]. Zheng and Luh later extended Mason's results by identifying one manipulator as the leader, and the other as the follower [4,5]. Kinematic constraints were also formulated in [4,5] for the leader and follower when they handled rigid objects as well as objects with degrees of freedom, such as a pair of pliers. Hemami [6], on the other hand, gave another approach to study the coordination control of two moving arms, in which the rigid body constraint equation was replaced by a symmetry relationship between the arms. More recently, Lee [7] extended the concept of the robot manipulability to redundant dual-arm systems. He pointed out that the required motion and force trajectories of a given task by a redundant dual-arm system could be abstracted by a series of desired manipulability ellipsoids. Furthermore, task-oriented dual-arm manipulability could be mathematically defined by quantifying how the manipulability of one arm affects the other and measuring the geometrical closeness between the desired and the actual manipulability ellipsoids.

Dynamics of two coordinating robots have also been extensively studied. In [8,9], it was revealed that two dynamic equations, one for each coordinating robot, could be combined to form one unified dynamic equation when the two robots were handling a rigid object. In the control aspects of two coordinating robots, Tarn, Bejczy and Yun [10,11] developed a nonlinear dynamic control method. The main feature of their method is that the nonlinear feedback mechanism was integrated with an optimal error correcting loop and an optimal coordinator. Ozguner, Yurkovich and Al-Abbass [12] established a hierarchical framework which employed two levels of control hierarchy. The decentralized model reference adaptive control approach using variable structure controller was applied. Hayati [13], and Yoshikawa and Zheng [14] extended the theory of hybrid position/force control to the case of multiple

coordinated robots. In [13], the solution was given by partitioning the object and considering the object as part of the last link of each arm, and cooperation was achieved by controlling each arm such that the burden of actuation was shared between the arms in a non-conflicting way. The method proposed in [14] could control the motion of the object as well as the forces exerted on the object. In another work, Koivo [15] proposed that the two coordinated robots could be controlled by an adaptive controller of a self-tuning type. The controller was designed on the basis of the stochastic multi-variable discrete time model, in which the system parameters were recursively estimated on-line by using a quadratic criterion.

While the studies on the coordination of multiple manipulators continue [16-20], one aspect has never received serious attention, i.e., handling deformable objects by multiple manipulators. In reality, however, there is a frequent occurrence of non-rigid objects. For instance, in the shipbuilding, aerospace, and automobile industries, flexible plates have long been used in the assembly of various kinds of vehicles. It is more noticeable in recent years that non-rigid composite materials such as pre-preg have been used to replace metal in many places [21]. Traditionally, to handle non-rigid materials, special toolings needed to be designed such as a vacuum pad [21]. The pads are designed to cover the most area of the object surface. When the space inside the pad becomes vacuum, the material can be picked up by the difference of the air pressure. However, such a mechanism needs a large pad when the object has a large surface area, which often becomes too large and too heavy to be carried by a robot manipulator. Human beings, on the other hand, can effectively handle large deformable objects with two hands. This reminds us that by coordinating two or more manipulators, it is possible to handle deformable objects by using ordinary end-effectors. As a result, large and heavy tools can be avoided. This, however, raises a new technical problem on coordination, i.e., how to coordinate motion trajectories of the two manupulators such that the deformable objects can be handled in an optimal way in terms of certain criteria? This problem will be studied in this paper.

In reality, there are three fundamental types of deformable objects, which are respectively, one, two, or three dimensional. The first two, however, occur more often than the third. Furthermore, two dimensional objects can often be treated as one dimensional when it is picked up by two manipulators. Consider a rectangular sheet picked up by two manipulators as shown in Fig. 1. If the sheet is picked up in such a way that the end-effectors are positioned at the center of the shorter dimension, the deformation is more likely to occur in the direction of

the longer dimension. Once the deformation occurs in one dimension, the deformation in the other dimension becomes negligible. As a result, two dimensional objects can be treated as one dimensional. For the reasons just cited, we concentrate our study on one dimensional objects, and the objects are simply called beams in the rest of the paper. We also assume that the deformation is elastic. That is, when the deformation force does not exist, the object is not deformed.

In the next section, we will define kinematic constraints for two coordinating manipulators when they handle an elastic beam. Since the beam is deformable, the relative position and orientation of the two manipulators are not necessary constant. Instead, the constraint relations can be described by inequality equations. This gives the two coordinated manipulators certain degrees of freedom in programming their motion trajectories. Their relative position and orientation can be modified to a certain extent to optimize some performance criteria. For example, when a flexible beam is folded and moved by two manipulators, the required workspace is smaller than when the beam is fully extended.

In the third section, we propose three methods for the two manipulators to handle an elastic beam. In the first method, the relative orientation can be altered, but not the position. In the second method, the relative position of the two end-effectors can be altered, but not the orientation. In the third method, both the relative position and orientation can be altered. Through the study of the object mechanics, the first method is quickly eliminated. Thus, the study concentrates on the second method. This method is investigated in terms of the magnitude of the forces and moments exerted on the objects and end-effectors. It is clear that in order to avoid any possible damage to the objects and heavy loads to the manipulators, the reaction forces and moments between the objects and end-effectors should be as small as possible.

In the fourth section, the study is concentrated on the third method. It is determined that the third method results in less reaction forces and moments than the second method. However, the motion trajectories of the end-effectors are more complex. In order to make the motion planning feasible in practical applications, we further propose an approximation approach. The behavior of the approximation approach is also analyzed.

In the fifth section, experimental results using both the second and third methods are presented. The paper is concluded by the sixth section, Conclusions.

2. KINEMATIC CONSTRAINTS ON TWO MANIPULATORS HANDLING A DEFORMABLE BEAM

In this section, we investigate kinematic constraints imposed on the relative position and orientation of two manipulators when they handle a flexible beam, for which the following review of notations of the manipulator kinematics is necessary.

According to the Denavit-Hartenberg convention [22], each link of a manipulator is assigned a coordinate system (x_i,y_i,z_i) for i=0,1,...,n, from the base link to the end-effector. The generalized coordinate, q_i, is the joint displacement of link i either rotating about or sliding along z_{i-1}. Let A_{i-1}^{i} be the 4 by 4 homogeneous transformation matrix which transforms a vector with reference to coordinates (x_i,y_i,z_i) to the same vector with reference to coordinates $(x_{i-1}, y_{i-1}, z_{i-1})$. Then one may have

$$A_0^n(q)=A_0^1(q_1)A_1^2(q_2)\cdots A_{n-1}^n(q_n) \tag{1}$$

where q is an n-dimensional vector consisting of n joint displacements $q_1,q_2,...,q_n$. A_0^n can be represented as follows

$$A_0^n(q)=\begin{bmatrix} n(q) & s(q) & a(q) & p(q) \\ 0 & 0 & 0 & 1 \end{bmatrix} \tag{2}$$

where n(q), s(q) and a(q) are unit vectors of coordinates x_n,y_n and z_n, respectively, and p(q) is position vector (Fig. 2). All vectors are with reference to the base coordinate. The orientation of the end-effector is specified by the 3×3 submatrix of $A_0^n(q)$:

$$R_0^n(q)=[n(q)\ s(q)\ a(q)] \tag{3}$$

Once the position and orientation vectors of the manipulator end-effectors are determined, the translational and angular velocities of the manipulator end-effectors v and ω can be derived

from p(q) and R_0^n (q) [22]. Then the robot joint velocities can be calculated from the following equation

$$\dot{q}=J^{-1}(q)\begin{bmatrix} v \\ \omega \end{bmatrix} \tag{4}$$

where J(q) is the Jacobian matrix.

We are now in a position to determine kinematic constraints imposed on the two manipulators which handle a flexible beam (Fig. 2). Consider two manipulators each with n joints. For convenience, one of the manipulators is named the leader and the other the follower. It is assumed that there are no relative motions among the end-effectors and the beam, and the length of the beam is inextensible.

Let (x_n^l, y_n^l, z_n^l) and (x_n^f, y_n^f, z_n^f) be the coordinate systems of end-effectors of the leader and the follower, respectively. Let r^l be the vector with reference to (x_n^l, y_n^l, z_n^l) (Fig. 2). Then the holonomic constraints on the relative position between the two robots can be written as in [4, 5]

$$p(q^l)+R_0^n(q^l)r^l-p(q^f)=0. \tag{5}$$

From (5), one may have

$$p(q^f)-p(q^l)=R_0^n(q^l)r^l \tag{6}$$

Since the beam is flexible, the distance between the two end-effectors, i.e., r^l is not a constant. As a result, one may obtain the following inequality equation from (6):

$$r_{min}<|p(q^f)-p(q^l)|=\left|R_0^n(q^l)r^l\right|=|r^l|<r_{max} \tag{7}$$

where $|r^l|$ represents the length of vector r^l, and r_{min} and r_{max} are the minimim and maximum length of $|r^l|$. It is clear r_{max} must be less than or equal to the total length of the beam.

Otherwise, either the beam is torn apart or the contacts between the beam and the end-effectors are lost, both of which are clearly not desired. To determine the minimum distance r_{min} is rather involved, which will be studied in section 3.

Eq.(7) reveals that when two manipulators are coordinated to handle a deformable object, either one or two dimensional, the manipulators have more motion freedom than when handling a rigid object. This motion freedom can be utilized to optimize other performance criterion of the manipulators. For example, avoid obstacles while handling the object, or reduce the required workspace when the object is large (to be realized by the reduction of the distance between the two end-effectors). etc. The detailed utilization of this advantage, however, will not be further addressed here.

In addition to the flexibility of the relative position, the relative orientation is also allowed to be modified in certain degree. The problem is how to formulate this motion freedom. Recall that when the object is rigid, the holonomic constraints for the orientation are [4, 5]

$$[R_0^n (q^l)]^T R_0^n (q^f) = U \tag{8}$$

where U is the constant matrix. When the two manipulators handle a flexible beam as shown in Fig. 2, we assume that twisting of the beam is not allowed. That is, $n(q^l)$ and $n(q^f)$ are always parallel. The holonomic constraints imposed on $n(q^l)$ and $n(q^f)$ can be described by the following equation

$$n^T(q^l)n(q^f)=1. \tag{9}$$

However, the relative orientation between the two vectors $a(q^l)$ and $a(q^f)$ can be modified, since the beam can be bent to a certain extent without being damaged. The holonomic constraints imposed on $a(q^l)$ and $a(q^f)$ can thus be depicted by the following inequality equation:

$$a_{min} < a^T(q^l)\, a(q^f) < a_{max}. \tag{10}$$

It is clear that a_{min} is equal to -1 which occurs when the beam has no deformation, and a_{max} is less than 1. When a_{max} is equal to one, the relative orientation of the two end-effectors is allowed to be zero. This will bend the beam as much as 90^0 by each end-effector.

In this section, we have defined kinematic constraints for two manipulators handling a deformable beam. It has been pointed out that the relative position and the orientation of the two end-effectors can be modified to a certain extent when handling deformable beams. How the modification can be made and what the relationship between the modifications of the positions and orientations remain unanswered. These topics will be studied in the following sections.

3. HANDLING A DEFORMABLE BEAM BY TWO MANIPULATORS WITH ONLY POSITION ALTERNATABLE

In this section, we investigate the strategies for handling a deformable beam by two manipulators. The strategies will define the limitations of r_{min} and a_{max} which appear in (7) and (10), as well as the relationship between the positional and orientational modifications.

From the discussion of the previous section, it can be easily found that three methods are theoretically possible to handle a flexible beam. They are:

Method A: the relative orientation is allowed to change, but the relative position is not.
Method B: the relative position is allowed to change, but the relative orientation is not.
Method C: both the relative position and the relative orientation are allowed to change.

With three methods proposed, it is natural to make comparison among them such that the best one can be determined. Before doing so, a careful look at Fig. 2 reveals that method A is impossible in reality. Since the beam is firmly grasped by the end-effectors, one cannot change the relative orientations without changing the relative positions unless the portions grasped by the end-effectors are torn off from the beam. The latter, however, is unrealistic. We therefore can eliminate method A and concentrate on methods B and C.

To evaluate methods B and C, we select the reaction forces and moments between the beam and the end-effectors as the criterion. This selection is based on the fact that the forces and moments are exerted on the beam when the beam is deformed, and should be as small as

possible. Small reaction forces and moments result in low external loads to the manipulators as well as low possibilities of damage to the objects. This consideration amounts to analyzing the deflection behavior of the beam under the external forces and moments for each method. In the rest of this section, we will study the method B. Method C will be investigated in the fourth section.

3.1 Deflection Behavior of the Beam when the Beam Has a Small Deflection

In this subsection, we analyze the deflection behavior of the beam when the beam has a small deflection. It is first assumed that the beam is weightless. This assumption is based on the consideration that we are dealing with deformable beams whose deformation caused by the beam weight is relatively small. Only when external forces and moments are exerted on the beam ends, will deformation become large. In reality, many deformable objects have this characteristic, a practical example of which will be shown in the experimental studies.

Consider a beam held by the end-effectors at its two ends. For convenience, we call the line that connects the two end points of the beam the reference line. When the beam completely lies on the reference line, no deflection occurs. If the two end-effectors move towards each other on the reference line with the orientation unchanged, the beam starts to be deformed. According to classic mechanics [23, 24], the beam can be deformed in two different cases. Fig. 3 shows the first case in which the deformation has only one buckle, and Fig. 4 shows the second case in which the deformation has two buckles [23, 24].

In case 1, the beam is deflected to form a curve in the center, but the beam ends are still aligned in the same directions of the end-effectors. In doing so, two infection points appear on the beam. The curvatures at the infection points are zero; therefore, no moments are exerted on the infection points. Thus the infection points are also called the points of zero moment (ZM) [23, 24]. It is also pointed out in [24] that the points of ZM occur at approximately the quarter points of the beam (Fig. 3).

Now just consider the portion of the beam between the two points of zero moment. Its length is one half of the entire beam. Since the points of ZM do not provide any moment to the beam, the points behave as hinges (recall that the hinges do not provide moments to the beam but only the forces). Thus, the portion between the two points of ZM behaves as a hinged-

hinged beam. For a hinged-hinged beam, however, the relationship between the external force and the deflection is well defined (Appendix 1 of this paper provides the details). It can be shown that if the deflection of the beam is small, the force exerted on the point of ZM can be expressed as

$$F_{1S} = \frac{\pi^2 EI_z}{(L/2)^2} = \frac{4\pi^2 EI_z}{L^2} \tag{11}$$

where E is the stiffness of the beam material, I_z the moment of inertia of the cross-section of the beam with respect to axis z, and L the length of the beam. Since the deformation is static once the distance between the two end-effectors becomes constant, the end-effector has to provide the same force, i.e., F_{1S} to the beam end. In addition, if the deflection of the hinged portion is δ, the total deflection of the beam will be 2δ [23, 24] (Fig. 3). That is, the distance from the point of ZM to the reference line is δ. As a result, the moment that is exerted on the end-effectors can be expressed as

$$M_{1S} = F_{1S}\delta = \frac{4\pi^2 EI_z \delta}{L^2} \tag{12}$$

Note that the deflection parameter δ is very small in a small deflected beam, and no formulation is provided to calculate it. In the large deflection case, δ is no longer negligible, and needs to be specifically calculated. This topic will be further addressed later.

In case 2, it is found[24] that the points of ZM (i.e. the hinges) occur at approximately $\frac{L}{2}$ and $\frac{0.7L}{2}$ points, as shown in Fig. 4. Hence the portion of length $\frac{0.7L}{2}$ is in effect a hinged-hinged beam. The behavior of the hinged-hinged beam in this case is also provided in Appendix 1, and we find the force exerted on the hinge to be:

$$F_{2S} = \frac{\pi^2 EI_z}{(0.7L/2)^2} = \frac{8\pi^2 EI_z}{L^2} \tag{13}$$

From (13) and Fig. 4, one can also obtain that the force exerted on the end-effector is F_{2S}, and the moment exerted on the end-effector is:

$$M_{2S} = \frac{8\pi^2 EI_z \delta}{L^2} \qquad (14)$$

Since δ is not specified in (12) and (14), the absolute value of M_{1S} and M_{2S} can not be calculated unless one knows the exact deflection in reality. However, equations (11) - (14) reveal that for the same amount of deflection, case 1 results in less forces and moments exerted on the end-effectors. Therefore, case 2 should be avoided in practice.

In reality, if the beam is originally grasped by the end-effectors with no deflection, and the end-effectors start to approach to each other on the reference line, case 1 will always occur first. This is because the deformation forces and moments gradually grow as the distance between the end-effectors decreases, and case 1 needs less forces and moments than in case 2. Once case 1 occurs, case 2 will never occur. On the other hand, if the two end-effectors are off the reference line, i.e., the two vectors, a(q), of the end-effectors are not aligned on the same line, case 2 may occur first (Fig. 5). Therefore, to avoid case 2, one should maintain the two end-effectors on the same reference line when they are approaching to each other.

3.2 Deflection Behavior of the Beam when the Beam Has a Large Deflection

The results obtained in the previous subsection are for small deflections. In the small deflection case, the distance between the two end-effectors are virtually the same as the length of the beam. Therefore, the end-effectors do not have too much freedom in their motion. When the end-effectors are even closer to each other, the beam may have a large deflection. Although the forces and moments exerted on the end-effectors will be different in the large deflection case, the analysis of the forces and moments are still rooted in the small deflection case.

Introduce a fixed-free ended beam under large deflection as shown in Fig. 6. Note that one end of the beam is fixed on the wall and the other has a force F_{3L} exerted on it. It is shown in Appendix 1 that the behavior of this fixed-free ended beam is the same as the right half of a hinged-hinged beam under small deflections. The convenience of this introduction,

however, will be soon made clear. It is shown in [24] that for large deflections, the force exerted on the hinge can be obtained from the following equation:

$$\frac{F_{3L}}{F_3} = \left(\frac{2R(\alpha)}{\pi}\right)^2 \tag{15}$$

where F_3 is the force exerted on the end of a fixed-free ended beam when the deformation is small, and its value can be calculated using the formulation described in Appendix 1. In (15) $R(\alpha)$ is obtained from the following integral:

$$R(\alpha,\phi_1) = \int_0^{\phi_1} \frac{d\phi}{\sqrt{1-k\sin^2\phi}} \tag{16}$$

where $k=\sin^2(\alpha/2)$, angle α is the deflection angle as shown in Fig. 6. When $\phi_1=\frac{\pi}{2}$, (16) gives $R(\alpha)$. Also, for large deflections, the exact deflection, δ, can be calculated by the following equation:

$$\frac{\delta}{L_1} = \frac{2}{R(\alpha)}\sin(\alpha/2) \tag{17}$$

where L_1 is the length of the beam. Furthermore, the distance, r_1, can be obtained from

$$\frac{r_1}{L_1} = \frac{2P(\alpha)}{R(\alpha)} - 1 \tag{18}$$

where $P(\alpha)$ can be calculated from another elliptic integral:

$$P(\alpha,\phi_1) = \int_0^{\phi_1} \sqrt{1-k\sin^2\phi}\, d\phi. \tag{19}$$

From (19), one may have $P(\alpha) = P(\alpha,\phi_1)\big|_{\phi_1=\frac{\pi}{2}}$.

With the forthgoing analysis of the fixed-free ended beam, we can now further evaluate Method B. From Fig. 3, it can be seen that in case 1, the entire beam can be divided into four pieces of fixed-free ended beam, separated by the points of ZM. Starting from the left, the first piece is from the left end-effector to the first point of ZM (consider that the end-effector as the fixed point), and the second piece is between the first point of ZM and the center point (the center point can be considered as the fixed point), etc. For every piece, we can determine the hinged force F_{3L}, the deflection δ and the distance r_1, from the deflection angle α (here α is the same as θ shown in Fig. 3) using (15), (17) and (18). It should be noted that L_1 in (17) and (18) is equal to $\frac{L}{4}$. It is clear that the hinged force is also the force exerted on the end-effector. The total deflection of the beam, however, is twice as much as the calculated deflection δ, and the distance between the two end-effectors, $|r'|$, is four times as much as r_1.

Based on the above discussion, the behavior of the large deflection beam, as shown in Fig. 3, can be expressed as follows (here F_{1L}, the force under large deflection, is used instead of F_{1S})

$$F_{1L}=\frac{(4R(\alpha))^2 EI_z}{L^2} \tag{20}$$

$$|r'| = L(\frac{2P(\alpha)}{R(\alpha)} - 1) \tag{21}$$

and the deflection of the beam is equal to

$$2\delta = \frac{L}{R(\alpha)} \sin(\frac{\theta}{2}). \tag{22}$$

The moment exerted on the end-effector can be calculated as

$$M_{1L} = F_{1L}\delta. \tag{23}$$

One may note that the evaluation of (20) to (22) involves the computation of two elliptic integrals. But in reality, $R(\alpha)$ and $P(\alpha)$, corresponding to a certain deflection angle α, can be found from a well developed table which is provided by many textbooks of mathematics and mechanics. For example, the table shown in Appendix 2 is found in reference [25].

3.3 The Minimum Distance between the Two Grippers

With the results provided in the previous two subsections, we can further investigate the minimum distance between the two end-effectors. The criterion to determine the minimum distance r_{min} is based on two factors: the maximum stress that the deformable beam can withstand without being damaged, and the maximum load that the manipulators can carry. The procedure of the determination is as follows.

Consider a single piece ended by a ZM point and the end-effector in an entire beam (Fig. 3). It behaves as a fixed-free ended beam, for which the following relationship must always hold [24] .

$$\sigma_{direct}+\sigma_{bending}=\frac{F_{1L}}{A}+\frac{y_m F_{1L}\delta}{I_z} < \sigma_{max} \qquad (24)$$

where σ_{max} is the maximum allowable stress that the beam can withstand, σ_{direct} is the stress due to direct compression, and $\sigma_{bending}$ is the stress due to bending. A is the area of the cross section of the beam, I_z is the area moment of inertia with respect to axis z, and y_m is the distance from the center to the edge of the area where the bending occurs (Fig.7). Since both F_{1L} and δ are functions of the bending angle α, finding the minimum distance amounts to finding the angle α such that (24) is satisfied. However, because both the functions involve elliptic integrals, solving for α from (24) is rather complicated. Instead, we can use a trial-and-error method.

We may first arbitrarily select a deflection angle α. Based on α, F_{1L} can be calculated using (20), and the deflection δ can be calculated using (22). Substituting the calculated F_{1L} and δ into (24). If it can be satisfied, we further enlarge α; otherwise it should be reduced.

The same procedure is then tried again until a maximum deflection angle which satisfies (24) is found.

The hinged force and moments thus found still have to satisfy the load criterion of the manipulator. If M_{1L} and F_{1L} are less than the maximum capabilities of the manipulators, the selected deflection angle is acceptable. Otherwise, they have to be reduced. Basically, if the calculated force is greater than the capability of the manipulators, we have to use (20) to find the maximum value of $R(\alpha)$ (let F_{1L} be the capability of the manipulator), and further find the deflection angle from the lookup table. Likewise, (23) may be used to determine the deflection angle if the calculated M_{1L} is greater than the capability of the manipulator. Once the maximum deflection angle is found, one may use (21) to find the minimum distance that the two end-effectors can be at while handling a flexible beam.

4. HANDLING A DEFORMABLE BEAM BY TWO MANIPULATORS WITH BOTH ORIENTATION AND POSITION ALTERNATABLE

In the previous section, we have studied method B in which the end-effectors are only allowed to have position difference. In this section, we investigate method C in which both position and orientation alterations are permitted. It is clear that there are many possible combinations of the relative position and orientation between the two end-effectors. However, not all of them are suitable for handling deformable beams. We should first select the best combination from all the possibilities. Then the minimum distance and the maximum orientation difference between the two end-effectors can further be investigated.

4.1 The Best Combination of the Relative Position and Orientation

To determine the best combination, we again use the force and moment criterion, i.e, minimizing the force and moment exerted on the end-effectors as well as on the objects. To do so, we propose and prove the following claim.

Claim: When the two end-effectors grasp the beam in such a way that the two end points of the beam coincide with the ZM points of the beam, and the orientation of the end-effectors are

the same as the deflection angle of the beam (Fig.8), the end-effectors suffer the minimum forces and moments.

Proof: We prove this claim for the forces and the moments, respectively, as follows. From the discussion of the previous section, it can be seen that the force exerted on the ZM point is related to the length of the portion between the two ZM points. Longer length results in small forces in both the small and large deflection cases (see (11) and (20)). It follows that if the two end points of the beam are at the ZM points while the beam is bent, the end points will behave as hingers. Since the length of the beam is the maximum distance that the portion between the two hinge points could be, the force exerted on the hinge points or the center of the end-effectors (assume that the center of the end-effectors coincide with the end points of the beam) becomes the minimum.

Next we consider the moments exerted on the end-effectors. Since the orientations of the end-effectors coincide with the deflection angle of the beam, the curvature of the beam at the tip of the end-effectors are null. If the curvature is zero, it follows from the following formulation, which describes the deformation behavior of a elastic beam [23,24],

$$\frac{1}{\rho} = \frac{M}{EI_z} \tag{25}$$

that the moments exerted on the end-effectors are zero, where $\frac{1}{\rho}$ is the curvature of the beam. Any deviation of the end-effectors orientation from the deflection angle will result in non-zero curvature which will generate bending moments exerted on the end-effectors. ♦

With the claim just proved, we can further consider the minimum distance and the maximum orientation difference between the two end-effectors. This will be discussed in the following subsection.

4.2 The Minimum Distance and the Maximum Orientation Difference between the Two End-Effectors

The procedure applied in subsections 3.2 and 3.3 can be used again here. The beam now behaves as two pieces of fixed-free ended beam (Fig. 8). The parameters associated with the

deformation can be respectively calculated as follows. First, the exerted force can be written as:

$$F_{4L} = \frac{(2R(\alpha))^2 EI_z}{L^2} . \tag{26}$$

Then, the distance between the two end-effectors can be calculated using:

$$|r^l| = L(\frac{2P(\alpha)}{R(\alpha)} - 1), \tag{27}$$

and the deflection of the beam is equal to:

$$\delta = \frac{L}{2R(\alpha)} \sin(\frac{\alpha}{2}) . \tag{28}$$

The minimum distance between the two end-effectors can be determined using the procedure as outlined in subsection 3.3 using (26), (27) and (28) instead of (20), (21) and (22). Essentially, one needs to find a maximum deflection angle, α_{max}. Once α_{max} is found, not only the minimum distance can be found by using (27), but also the maximum orientation difference can be obtained as:

$$a^T(q^l)a(q^f) \leq a_{max} = \cos(2\alpha_{max}). \tag{29}$$

In reality, however, the exact value of the maximum stress is often not known; therefore, mathematical computation of the minimum distance and the maximum orientation difference may not be possible. In this case, we may have to practically bend the beam until the limit is reached. In this regard, specifying the trajectories of the end-effectors while they are bending the beam becomes a more important issue than finding the maximum orientation difference. This topic will be discussed in the next subsection.

4.3 The Relationship between the Positions and Orientations of the End-Effectors while Bending the Beam

For simplicity, we concentrate our discussion on a single end-effector which is shown on the right side of Fig. 8. Assume that when the end-effector picks up the beam, the beam is not deformed, and the position and orientation of the end-effector is $[x, y, \alpha] = [0, 0, 0]$. From the discussion of the previous subsection, it can be found that the trajectory of the end-effector can be expressed as:

$$\begin{cases} x(\alpha) = L\left(\dfrac{P(\alpha)}{R(\alpha)} - \dfrac{1}{2}\right) \\ y(\alpha) = \dfrac{L}{R(\alpha)}\sin(\alpha/2) \end{cases} \tag{30}$$

Note that the x and y coordinates are complex functions of the end-effector orientation. Essentially, we can use the end-effector orientation as an independent variable, and linearly increase it as the end-effector bends the beam. The position of the end-effector can be calculated by using (30).

There are two practical problems involved in this method. First, the computation involved in (30) is rather complicated. It is practically impossible to execute the computation of (30) in real time by the manipulator controller. Secondly, even if the computation can be handled by the controller, for example by using a look-up table as shown in Appendix 2 (a much more detailed version is needed though), executing such a trajectory by the practical manipulators is very time consuming, since the manipulators have to execute point to point motion along the trajectory. Between every pair of points, the motions have to be interpolated by a complicated computation [25]. If one can reduce the intermediate points on the trajectory, the computation can be simplified, and the manipulator motion can be sped up.

In reality, we coarsely divide the desired trajectories of the two end-effectors into a few pieces. For example, every piece can cover about 10 degrees of the deflection angle. The positions of the two end points of each piece can be specified by (30) or using a look-up table. The motions between the two end points are simply linear. When using a PUMA manipulator,

this motion can be programmed by using the instruction MOVES D(n), where D(n) is the end point of the nth piece. The instruction means that the end-effector is linearly moved from the end point D(n-1) to D(n). Since the trajectory between any two end points are not obtained from (30) or a look-up table, the problem is how the force and moment situation will be affected by using this simple approximation method. This topic will be studied in the following subsection.

4.4 Behavior of the Approximation Method

For simplicity, we just consider one half of the entire beam. Assume that the end-effector moves along the trajectory specified by (30), and the grasping point is located at point Q on the trajectory which is a curve between the two end-points N and M (see Fig. 9). If we use the line segment between N and M, instead of the curve, as the trajectory, the grasping point will be at J as shown in Fig. 9. Without loss of generality, we assume that JQ is parallel to the axis x. When the grasping point moves from point Q to J, the shape of the beam is converted from OQ to be O'J as shown in Fig. 10, and the inflection points will occur on the beam instead at the end points of the beam. The question is where those infection points are since the positions of the infection points affect the forces and moments exerted on the end-effetors.

As mentioned in the previous section, the inflection point is the point of ZM, and the ZM points occur at the quarter points of the beam when the end-effectors are aligned on the same line. To take advantage of this conclusion, we extend the length of the original beam in such a way that the infection points of the original beam are also at the quarter points of the extended beam. Clearly, for the extended beam, the orientation of its two ends must be aligned on the same line. For the right half of the extended beam, the deformed shape is shown as curve O'H in Fig. 10. It should be noted that the original beam O'J is now a segment of the extended beam O'H. For the extended beam O'H, the results of the previous section can be used in our analysis.

Assume that the angle between the end-effector and JQ is φ, and the deflection angle at point G (i.e., ZM point) is α_x. For segment GH of the extended beam O'H, we may have the following relationships [24]:

$$\sin \phi_1 = \frac{\sin (\varphi/2)}{\sin (\alpha_x/2)} \tag{31}$$

$$t = L_x \left(\frac{2P(\alpha_x,\phi_1) - R(\alpha_x,\phi_1)}{R(\alpha_x)} \right) \tag{32}$$

and

$$s = L_x \left(\frac{R(\alpha_x,\phi_1)}{R(\alpha_x)} \right) \tag{33}$$

where L_x is one half of the length of the extended beam OH ; t and s are as shown in Fig.10 (also see Fig. 6), and the other terms have previously been defined. For the extended beam, (18) can now be written as:

$$\frac{r_x}{L_x} = \frac{2P(\alpha_x)}{R(\alpha_x)} - 1 \tag{34}$$

where r_x is as shown in Fig. 10.

From (32) and (34), we obtain the following expression for t :

$$t = r_x \left(\frac{2P(\alpha_x,\phi_1) - R(\alpha_x,\phi_1)}{2P(\alpha_x) - R(\alpha_x)} \right). \tag{35}$$

Let

$$C = r_x + (r_x - t) = 2r_x - t. \tag{36}$$

From Fig. 10 we also have

$$\frac{L}{2} = 2L_x - s \tag{37}$$

where L is the length of the original beam. Substituting (33) into (37), we obtain:

$$L_x = \frac{LR(\alpha_x)}{4R(\alpha_x) - 2R(\alpha_x,\phi_1)} \tag{38}$$

From (34), (35), (36), and (38), we obtain:

$$\frac{C}{L} = \frac{2P(\alpha_x) - P(\alpha_x,\phi_1)}{2R(\alpha_x) - R(\alpha_x,\phi_1)} - \frac{1}{2}. \tag{39}$$

From the discussion of subsection 4.2, it is known that if the grasping point is at Q, one has (see Fig.8 and (18)):

$$\frac{r_1}{L} = \frac{P(\alpha)}{R(\alpha)} - 1 \tag{40}$$

Let the length of JQ be Δ. C that is expressed by (36) can also be expressed as:

$$C = r_1 - \Delta \tag{41}$$

Using (40) and (41), (39) becomes:

$$\frac{\Delta}{L} = \frac{P(\alpha)}{R(\alpha)} - \frac{2P(\alpha_x) - P(\alpha_x,\phi_1)}{2R(\alpha_x) - R(\alpha_x,\phi_1)} \tag{42}$$

From the above discussion, one can see that if Δ and φ are specified, α_x can be calculated using (31) and (42). Δ is the position difference of the end-effector between points Q and J, and φ can be assumed to be the same as α (recall that α is an independent variable when programming the motion trajectory). Once α_x is calculated, one can proceed to find the forces and moments exerted on the end-effectors.

For the extended beam OH (Fig. 10), one can use (15) to determine the force F_x that is exerted on the point of ZM, G, to be:

$$F_x = \frac{(R(\alpha_x))^2 EI_z}{L_x^2}. \tag{43}$$

It is clear that the force F_x is also the force exerted on the end-effector.

When the grasping point is at the point Q, the exerted force F_{4L} can be calculated from (26). From (26), (38), and (43) we obtain the following relationship between F_x and F_{4L}:

$$\frac{F_x}{F_{4L}} = \left(\frac{2R(\alpha_x) - R(\alpha_x,\phi_1)}{R(\alpha)}\right)^2. \tag{44}$$

Since $R(\alpha_x)$ is greater than $R(\alpha_x,\phi_1)$ (the former is equal to the latter only when ϕ_1 is equal to $\pi/2$), and $R(\alpha_x)$ is greater than $R(\alpha)$, F_x is greater than F_{4L}. However, as long as Δ is small, the difference between F_x and F_{4L} is still manageable.

To calculate the moment exerted on the end-effector, we have to calculate the force arm, h, as shown in Fig. 10. From [24], it is known that the relationship between h and L_x as shown in Fig. 10 can be expressed as:

$$2L_x^2(\cos\varphi - \cos\alpha_x) = ((R(\alpha_x))^2 h^2 \tag{45}$$

Substituting L_x in (45) by (38), the force arm can be written as:

$$h = \frac{L\sqrt{2(\cos\varphi - \cos\alpha_x)}}{2(2R(\alpha_x) - R(\alpha_x,\phi_1))} \tag{46}$$

Consequently, the moment exerted on the end-effector can be written as $F_x h$ and calculated by using (43) and (46). It should be emphasized that the moment is a completely new addition to the total forces and moments that are exerted on the end-effector.

To summarize the discussion presented so far in this section, it can be seen that because of the position difference caused by using the line segment to approximate the trajectory curve, the forces and the moments exerted on the end-effectors are enlarged. If it is necessary, the exact values of the forces and moments can be calculated by using the formulations that have just been defined. In the next subsection, we will use a numerical example to illustrate how the forces and moments are affected by the position difference of the end-effectors.

4.5 Numerical Example for the Approximation Method

Consider that the arc, MN, in Fig. 9 is the trajectory of an end-effector specified by (30). With the specified trajectory, the end-effector bends the beam from $\alpha = 0^\circ$ to $\alpha = 10^\circ$. The equation for the line segment MN can be expressed by is:

$$\frac{x - \frac{L}{2}}{x(10^\circ) - \frac{L}{2}} = \frac{y}{y(10^\circ)} \tag{47}$$

where $x(10^\circ)$ and $y(10^\circ)$ can be calculated by using (30).

We now assume that at point Q, $\alpha = 5^\circ$, which is in the middle of the bending process. The reason for selecting 5° is that at the middle point, the difference between point Q and point J is close to be the maximum, and the forces and moments are close to the maximum as well.

The coordinates of point Q can be calculated from (30). That is:

$$\begin{cases} x(5^\circ) = L\left(\dfrac{P(5^\circ)}{R(5^\circ)} - \dfrac{1}{2}\right) \\ y(5^\circ) = \dfrac{L}{R(5^\circ)} \sin(5^\circ/2) \end{cases} \tag{48}$$

The coordinates of point J, on the other hand, can be calculated as:

$$\begin{cases} x_J = \dfrac{L}{2} + \dfrac{y(5^\circ)}{y(10^\circ)} \left(x(10^\circ) - \dfrac{L}{2}\right) \\ y_J = y(5^\circ) \end{cases} \tag{49}$$

Once $x(5^\circ)$ and x_J are calculated, the difference, Δ, can be expressed as:

$$\Delta = x(5^\circ) - x_J \tag{50}$$

The numerical values are calculated as follows:

$$\frac{\Delta}{L} \approx 8.9193 \times 10^{-4}, \alpha_x \approx 5.5^0, \frac{F_x}{F_{4L}} \approx 1.63, \text{ and } \frac{h}{L} \approx 0.01.$$

It can be seen that the force exerted on the end-effector, F_x, is 1.63 times as much as F_{4L} due to the difference Δ. If the trajectory represented by the curve, MN, is approximated by more but shorter line segments, the force and the moment can be reduced.

5. EXPERIMENTAL STUDY

To verify the theoretical results, we have conducted experiments in our laboratory. The setup of the experiement is as shown in Fig. 11. Basically, in the experiment, a large number of elastic sheets needed to be assembled together to form a book. The book is then to be laminated to form a board. This assembly procedure is typical in the manufacturing of a Printed Wiring Board (PWB). Since each sheet has delicate circuits printed on the surface, and the circuits on multiple surfaces must be precisely aligned (within 0.001 inch), the assembly of the book is not a simple issue.

For the alignment purpose, each sheet has four positioning holes. Those holes are used to align the sheet with pins which are fixed on a base-board, which is used to hold the book (Fig.11). Since the tolerance between the pin and the hole is very tight, it is difficult to align all the holes with the pins at the same time. Instead, in the assembly process, the manipulators bend the sheet, such that the two middle holes can make contact with the pins first. Once the middle holes are aligned with the middle pins, the manipulators extend the sheet such that the remaining holes are aligned with the pins. In this process, the two manipulators first bend the sheet, following the trajectories that have to be specified using the methods defined in the previous sections, and come back to their original positions using the same trajectories.

We have tested both method B and method C in the experiment. In each method, the required bending angle was 40^o. From the table shown in Appendix 2, we can see that the distance between the two end-effectors needs to be reduced by about 12%. Since the dimension of the sheet was 18 by 12 inches, and the end-effectors held the center of the short sides, this reduction was equivalent to 2.1 inches. The experiment was conducted using an aluminum sheet (it was used to cover and protect the PWB during the lamination process). When method B was used, we

found that some permanent damage was made near the tip of the end-effectors. This is because method B imposes a large force and bending moment on the end-effector as discussed earlier. This clearly shows that method B was not adequate to bend the elastic sheet.

We then turned to method C. In programming the motions of the end-effectors, we divided the 40° deflection into four small pieces with 10° in each piece. Using the look-up table as shown in Appendix 2, we specified the positions of the end-effectors at the end points of the pieces, and used those points as the destination points for the end-effectors to move. Using the MOVES instructions as mentioned earlier, the end-effectors executed a piece-wise linear motion to move the two end-effectors to their final destination points at which the sheet was bent by 40°. By using method C the assembly was successfully completed without any damage to the aluminum sheet (Fig. 12).

6. CONCLUSIONS

In this paper we have discussed the mechanism for two coordinated manipulators to automatically handle deformable objects. After the kinematic constraints were analyzed for the manipulators, we investigated the coordinating methods for the two manipulators. In this respect, the main contributions can be summarized as follows:

(1) We have identified two coordinating methods for the two manipulators to handle one-dimensional objects. The first method only allows the relative position to be altered between the two end-effectors. The second method allows both relative position and orientation to be altered. From the analysis, we identified that the second method is better than the first method.

(2) For the second method, we further specified the end-effector trajectories, while they are bending an elastic sheet. The trajectories, however, were very complicated to compute. We further developed an approximation method, which used piece-wise linear segments to substitute for the trajectories. Furthermore, the behavior of the approximation method was also analyzed. Finally, experimental results were given to prove that the second method as well as the approximation of the method were effective for handling deformable objects.

REFERENCES

1. M.S. Konstantinov and M.D. Markov, "Two-hand robots for sophisticated manipulations in relative space," Proc. 10th Inter. Symp. Indust. Robots, Milan, Italy, March 5-7, 1980, pp.475-480.
2. E. Freund,"Hierarchical nonlinear control for robots," in Robotics Research-First International Symposium, Edited by M. Brady and R. Paul, MIT Press, 1984, pp.817-840.
3. M.T. Mason, "Compliance and force control for computer controlled manipulators," IEEE Trans. on System, Man and Cyber. Vol.SMC-11, N.6, June 1981, pp.418-432.
4. J.Y.S. Luh and Y.F. Zheng, "Constrained relations between two coordinated industrial robots for motion control," Int. J. of Robotics Research, Vol.6, No.3, Fall, 1987, pp.60-70.
5. Y.F. Zheng and J.Y.S. Luh, "Control of two coordinated robots in motion," Proc. IEEE 24th CDC, Fort Lauderdale, FL, Dec.11-13, 1985, pp.1761-1765.
6. A. Hemami, "Kinematics of two arm robots," IEEE Trans. Robotics and Autom., Vol.RA-2, No.4, Dec. 1986, pp.225-228.
7. S. Lee, "Dual redundant arm configuration optimization with task-oriented dual arm manipulability," IEEE Trans. Robotics and Autom., Vol.RA-5, No.1, Feb. 1989, pp.78-97.
8. Y.F. Zheng and J.Y.S. Luh, "Joint torques for control of two coordinated moving robots," Proc. 1986 IEEE Int. Conf. on Robotics and Automation, San Francisco, CA, April 7-10, 1986, pp.1375-1380.
9. N.H. McClamroch, "Singular systems of differential equations as dynamic model for constrained robot systems," Proc. 1986 IEEE Int. Conf. on Robotics and Automation, San Francisco, CA, April 7-10, 1986, pp.21-26.
10. T.J. Tarn, A.K. Bejczy and X. Yun, "Coordinated control of two arm robots," Proc. 1986 IEEE Int. Conf. on Robotics and Automation, San Francisco, CA, April 7-10, 1986, pp.1193-1198.
11. T.J. Tarn, A.K. Bejczy and X. Yun, "Dynamic coordination of two robot arm," Proc. IEEE 25th CDC, Athens, Greece, Dec. 10-12, 1986, pp.1267-1270.

12. U. Ozguner, S. Yurkovich and F. Al-Abbass, "Decentralized variable structure control of a two-arm robotic system," Proc. 1987 IEEE Int. Conf. on Robotics and Automation, Raleigh, NC, March 31-April 3, 1987, pp.1248-1254.
13. S. Hayati, "Hybrid position/force control of multi-arm cooperating robots," Proc. 1986 IEEE Int. Conf. on Robotics and Automation, San Francisco, CA, April 7-10, 1986, pp.82-89.
14. T. Yoshikawa and X. Zheng, "Coordinated dynamic hybrid position/force control for multiple robot manipulators handling one constrained object," Proc. 1990 IEEE Int. Conf. on Robotics and Automation, Cincinnati, Ohio, May 13-18, 1990, pp.1178-1183.
15. A.J. Koivo, "Adaptive position-velocity-force control of two manipulators," Proc. IEEE 24th CDC, Fort Lauderdale, FL, Dec.11-13, 1985, pp.1529-1532.
16. C.O. Alford and S.M. Belyeu, "Coordinated control of two robot arms," Proc. 1984 IEEE Int. Conf. on Robotics, Atlanta, GA, March 13-15, 1984, pp.468-473.
17. G. Hirzinger and J. Dietrich, "Multisensory robots and sensor based path generation," Proc. 1986 IEEE Int. Conf. on Robotics and Automation, San Francisco, CA, April 7-10, 1986, P.1992-2001.
18. R. Guptill and P. Stahura,"Multiple robotic devices: position specification and coordination," Proc. 1987 IEEE Int. Conf. on Robotics and Automation, Raleigh, NC, March 31-April 3, 1987, pp.1655-1659.
19. Y.F. Zheng, J.Y.S. Luh and P.F. Jia, "Integrating two industrial robots into a coordinated system," Computer in Industry, Vol.12, 1989, pp.285-298.
20. J.M. Tao, J.Y.S. Luh and Y.F. Zheng, "Compliant coordination control of two moving industrial robots," IEEE Trans. Robotics and Autom., Vol.RA-6, No.3, 1990, pp. 322-330.
21. D.E. Ruth and P. Mulgaonkar, "Robotic lay-up of prepreg composite plies," Proc. 1990 IEEE Int. Conf. on Robotics and Automation, Cincinnati, Ohio, May 13-18, 1990, pp.1296-1300.
22. J. Denavit and R.S. Hartenberg, "A kinematic notation for lower pair mechanics based on matrices," ASME Trans. Journal of Applied Mechanics, June, 1955, pp. 215-221.
23. R. Frisch-Fay, Flexible Bar, Washington Butterworths, 1962.
24. S.F. Borg, Fundamentals of Engineering Elasticity, D. Van Nostrand Company, Inc. 1962.
25. B.O. Peirce, A Short Table of Integrals, Ginn and Company, 1956.

Appendix 1

Consider a hinged-hinged beam (Fig. A-1) that is weightless and with a uniform EI_z, and the length of which, L_2, is inextensible. According to Bernoulli-Euler law under the condition of small deflection, we may have [23, 24]:

$$\frac{d^2v}{dx^2} = -\frac{M}{EI_z} \tag{A-1}$$

where v is the deflection in the direction y, M is the bending moment at any point t on the beam, and EI_z is the beam stiffness. In Fig. A-1, F is a horizontal force exerted on the end of the beam, and $\delta = v_{max}$.

In this case, one has:

$$M = Fv. \tag{A-2}$$

Thus (A-1) becomes

$$\frac{d^2v}{dx^2} = -\frac{Fv}{EI_z}. \tag{A-3}$$

Let

$$\frac{F}{EI_z} = K^2. \tag{A-4}$$

Eq. (A-3) can be written as

$$\frac{d^2v}{dx^2} + K^2v = 0. \tag{A-5}$$

Now we verify that

$$v = C_1 \sin Kx \tag{A-6}$$

satisfies equation (A-5), where C_1 is a constant, not equal to zero.

It is easy to see that the boundary conditions of the beam are

$$v = 0 \quad \text{at} \quad x = 0 \tag{A-7}$$

and

$$v=0 \quad \text{at} \quad x=L_2 . \tag{A-8}$$

The second boundary condition requires that

$$0=C_1 \sin KL_2 . \tag{A-9}$$

This condition will be satisfied only if

$$KL_2=n\pi, \qquad n=1,2, \ldots \tag{A-10}$$

By using Eq. (A-4), we can get

$$F=n^2\frac{\pi^2 EI_z}{L_2^2} . \tag{A-11}$$

Now consider two subcases:

subcase 1 (Fig A-2): when n=1, one has $F_1=\dfrac{\pi^2 EI_z}{L_2^2}$, and (A-12)

subcase 2 (Fig. A-3): when n=2, one has $F_2=\dfrac{4\pi^2 EI_z}{L_2^2}$. (A-13)

We can employ the results obtained so far to find solutions for other support conditions in the following manner. Consider a fixed-free ended beam as shown in Fig. A-4a. It has a length L_2 and a constant EI_z. In Fig. A-4b, we show a hinged-hinged beam of length $2L_2$ and with the same stiffness constant, EI_z, as the fixed-free ended beam. It can be seen that one-half of the hinged-hinged beam is identical to the fixed-free beam. Hence

$$F_3=\frac{\pi^2 EI_z}{(2L_2)^2} , \tag{A-14}$$

i.e.,

$$F_3=\frac{\pi^2 EI_z}{4L_2^2} . \tag{A-15}$$

Appendix 2

LOOK-UP TABLE FOR COMPUTING THE END-EFFECTOR POSITIONS

α (o)	R(α)	P(α)	$\frac{F_{3L}}{F_3}$	$\frac{\delta}{L_1}$	$\frac{r_1}{L_1}$
0	1.5708	1.5708	1.000	0	1
10	1.5738	1.5678	1.004	0.1116	0.9924
20	1.5828	1.55[illegible]	1.016	0.2193	0.9698
30	1.5981	1.5442	1.035	0.3239	0.9325
40	1.6200	1.5238	1.062	0.4221	0.8812
50	1.6490	1.4981	1.102	0.5126	0.8170
60	1.6858	1.4675	1.152	0.5930	0.7410
70	1.7312	1.4323	1.215	0.6626	0.6547
80	1.7868	1.3931	1.294	0.7195	0.5593
90	1.8541	1.3506	1.392	0.7625	0.4569

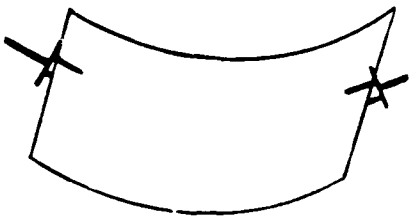

Fig. 1 A rectangular sheet picked up by two manipulators

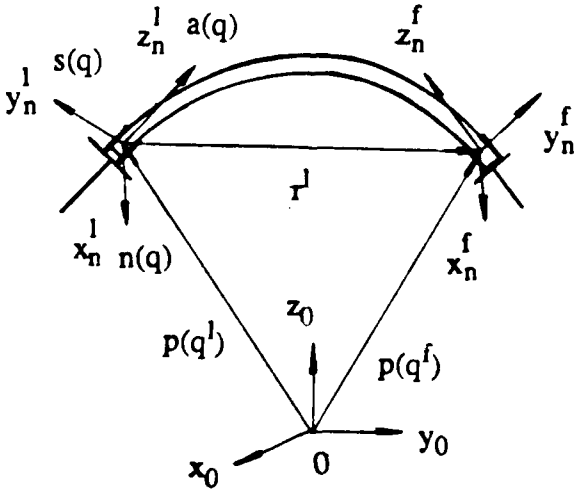

Fig. 2 The coordinate system and notations for two manipulators

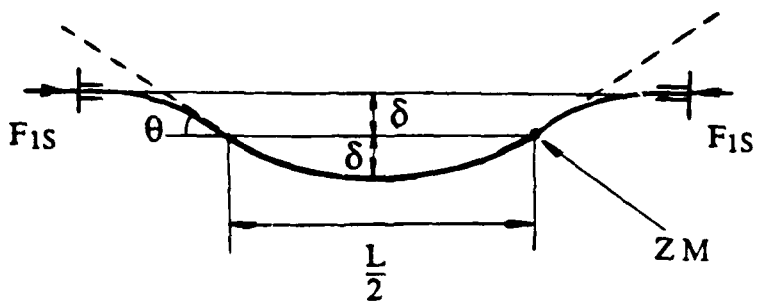

Fig. 3 The beam has one buckle in its deformation

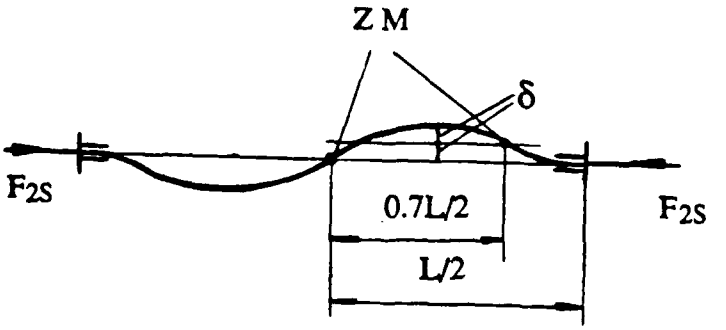

Fig. 4 The beam has two buckles in its deformation

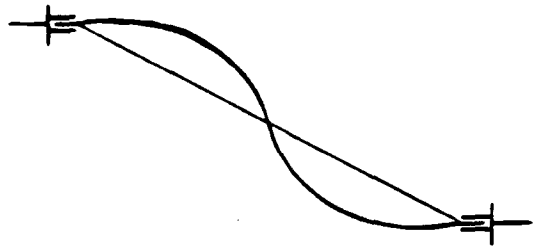

Fig. 5 Two grippers are not aligned on the same line, the deformation has two buckles

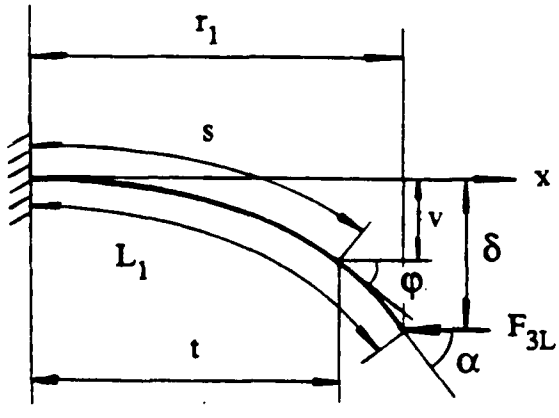

Fig. 6 A fixed-free ended beam under large deflection

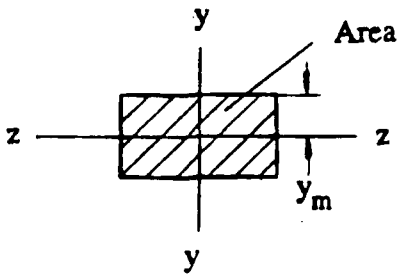

Fig. 7 The cross section of a beam

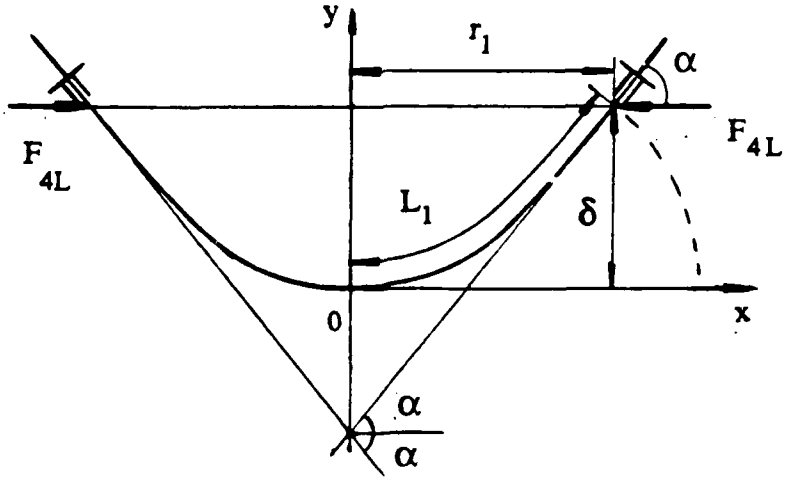

Fig. 8 The case of the minimum of the force and moment when the beam is bent

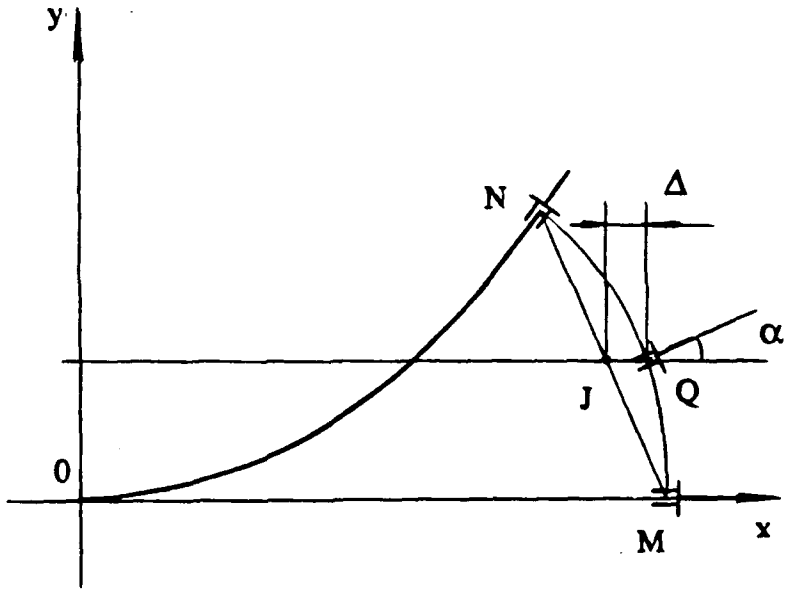

Fig. 9 The curve and the line segments of the end-effector trajectory

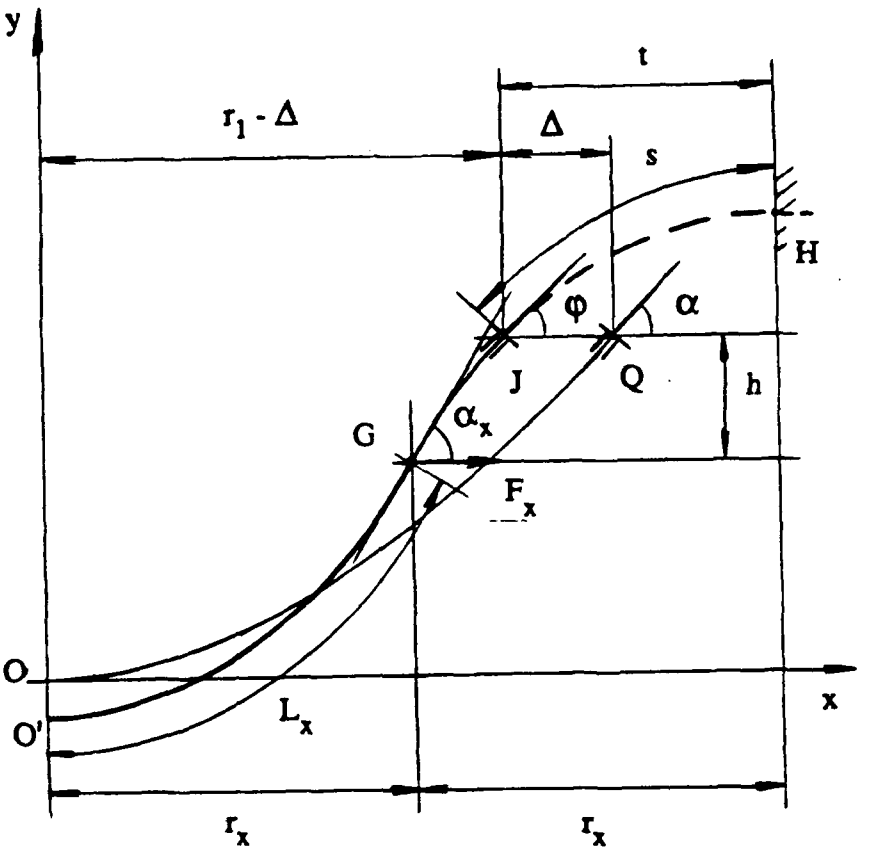

Fig. 10 Error analysis for the case of Fig.8

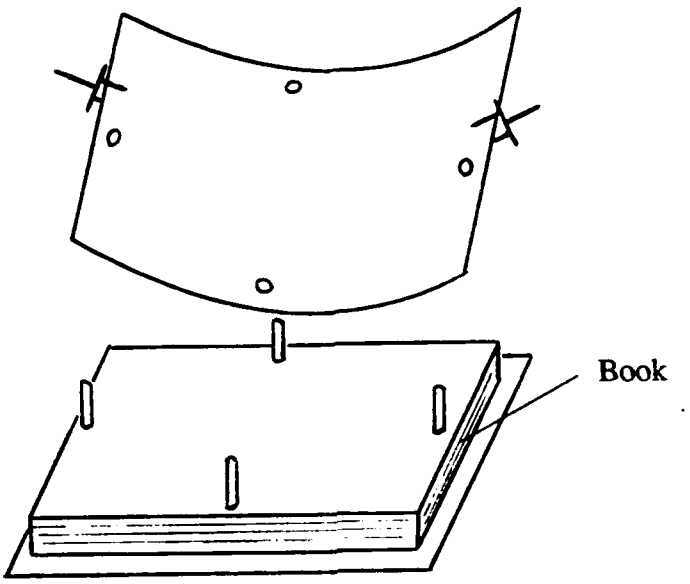

Fig. 11 The setup of the experiment

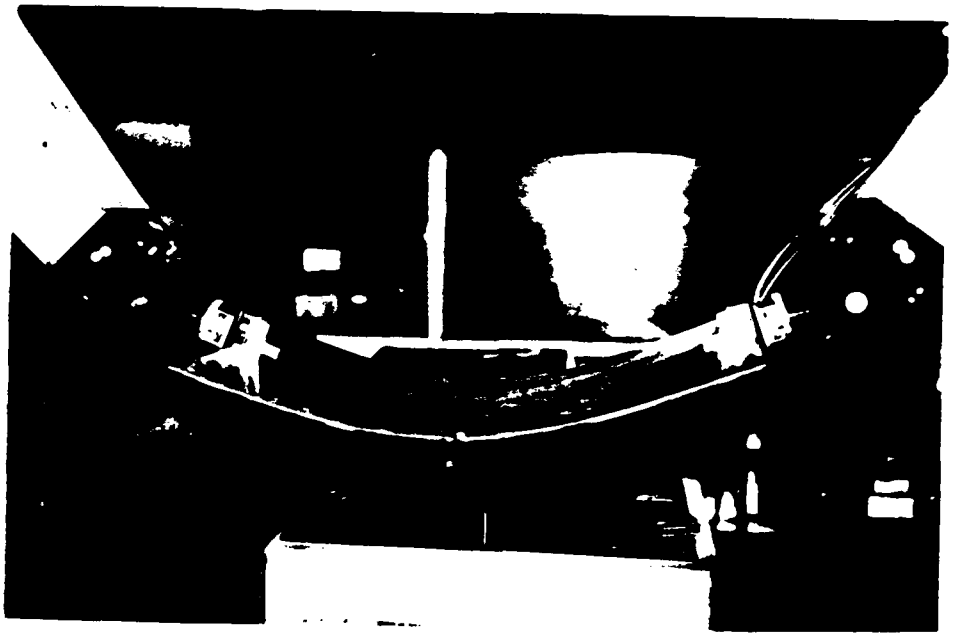

Fig. 12 The physical experiments

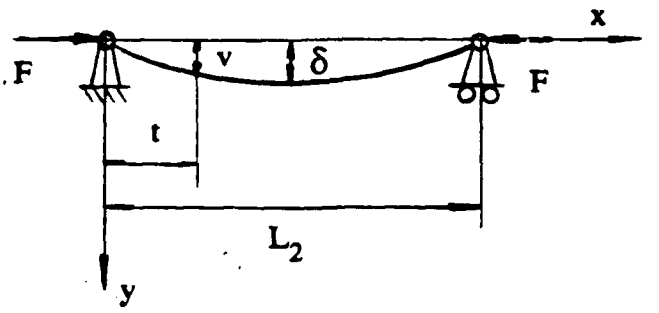

Fig. A-1 A hinged-hinged beam

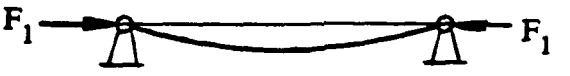

Fig. A-2 The beam has a deformation with one buckle

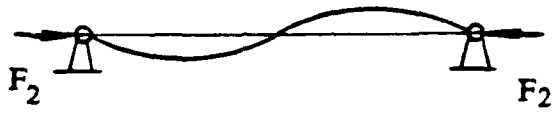

Fig. A-3 The beam has a deformation with two buckles

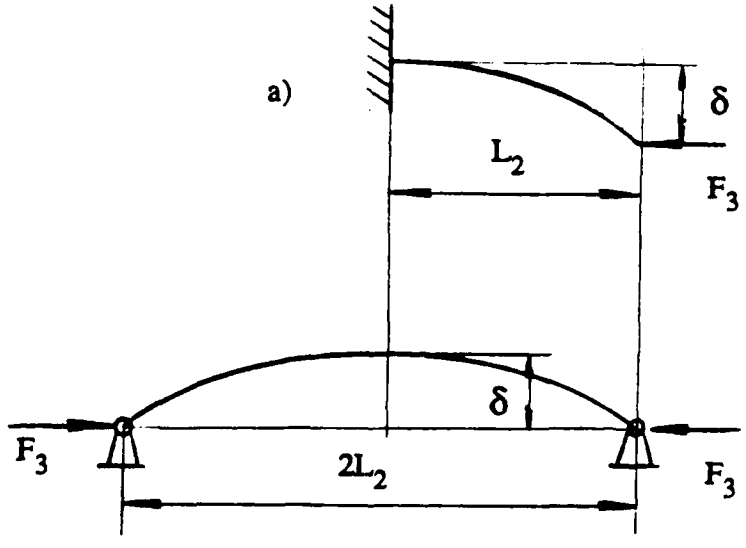

b)

Fig. A-4 A fixed-free ended beam under small deflection

Appendix B

Determination of the Third Dimension of an Object by Using a Range Finder

Rached Zantout & Prof. Yuan Zheng

I. Point Location Using a Range-Finder

The goal is to locate a point in space (i.e. know its x, y and z coordinates with respect to a reference frame) knowing only information about its image, captured by a Range-Finder.

The Range-Finder consists of a camera and a laser beam generator.

In the following, the system set-up and calibration will be described. Then a way to determine the coordinates of a point of interest is described. Finally, examples are given to prove the validity of the described algorithm.

Set-up and Calibration

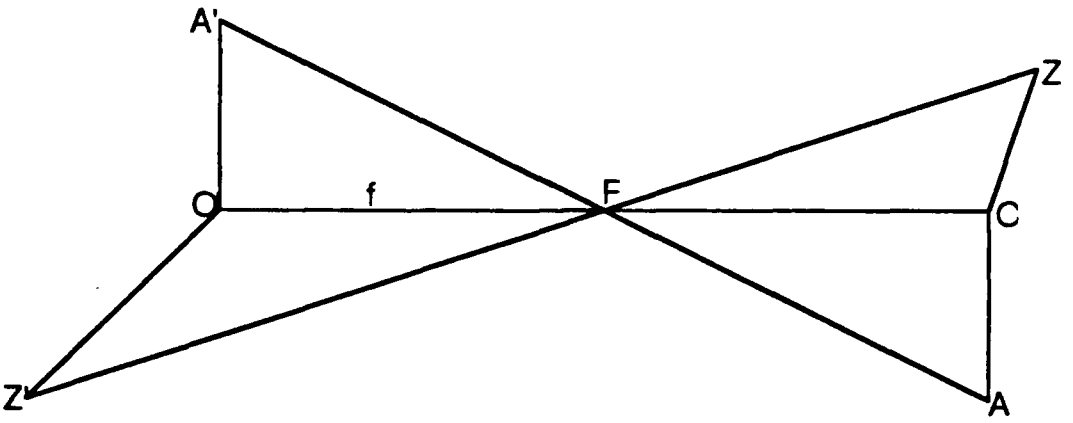

First, the camera and the Laser-beam generator are fixed and a reference frame is chosen such that its origin (O) is mapped to the middle of the screen (O'). The location of the camera $F(f_x, f_y, f_z)$, as well as the equation of the scanning plane $(Ax+By+Cz=D)$ are measured with respect to the reference frame. Then, a cube is put in front of the camera with one of its faces parallel to the camera's lens plane. A point (A) on that face is identified and the distance OA measured. On the screen, the distance between the images of those two points (O' and A') is also measured.

$$f = OF \times \frac{OA}{O'A'}$$

The orientation of the camera is then measured, and the parameters in the following equations are determined.

$$\mathbf{h} = h_x.\mathbf{x} + h_y.\mathbf{y} + h_z.\mathbf{z}$$

$$\mathbf{v} = v_x.\mathbf{x} + v_y.\mathbf{y} + v_z.\mathbf{z}$$

$$\mathbf{a} = a_x.\mathbf{x} + a_y.\mathbf{y} + a_z.\mathbf{z}$$

h and **v** define the coordinate frame of the image-plane.
a is the unit vector that is perpendicular to the image-plane.
h, **v**, and **a** pass through F and are the image-plane frame.
j_i is the projection of vector j on axis i.

In the case of calibration (and to make the calculations easier) the image-plane frame is taken to be at (-|**OF**|) on the y-axis from the reference frame. The orientation of both frames being the same.

Locating a Point of Interest

First, using a vision processor, the location of the image point is determined with respect to the **h**.**v** frame. The **h** component is "u" and the **v** component is 'v'. These coordinates are then transformed to reference-frame coordinates by applying the following:

$$p_x = u.h_x + v.v_x + f.a_x + F_x$$

$$p_y = u.h_y + v.v_y + f.a_y + F_y$$

$$p_z = u.h_z + v.v_z + f.a_z + F_z$$

The line on which the point of interest lies has the following parametric equation:

$$x = F_x + (p_x - F_x).t$$

$$y = F_y + (p_y - F_y).t$$

$$z = F_z + (p_z - F_z).t$$

The point of interest "R" is located on the intersection of the scanning-plane with the above line (since we already know that the point of interest is on the laser line). Combining the scanning-plane equation with the equation of the above line, we get:

$$t = \frac{(D - (a.Fx + B.Fy + C.Fz))}{((A.px + B.py + C.pz) - (A.Fx + B.Fy + C.Fz))}$$

Replacing this value of "t" in the equations for the line above, we get the coordinates of the point of interest.

Examples

The following coordinates were obtained through physical measurement:

F(0,-41,0)
B(0,0,0)
A(5.1,0,0)
C(5.1,0,-2.8)

On the screen, the images of A, B, and C were at (84,0), (0,0), (84,-38).

From the above data:

$$f = BF \times \frac{A'B'}{AB} = 41 \times \frac{84}{5.1}$$

the line (A'F) will have the following equation:

$$x = -84*t$$

$$y = -41 - 675.294*t$$

$$z = 0$$

Knowing that C is on the plane (y = 0), then it is on the intersection of that plane with the line (A'F). Applying this will give us:

$$t = -0.061$$

then the coordinates of the point C were calculated to be:

$$x = 5.124$$

$$y = 0$$

$$z = -2.318$$

We remark here a discrepancy between the calculated and the measured values for the coordinates of the point C. This is due to the poor measuring instruments that were used during the experiment. Still if we eliminate all these errors, there will always be an error due to the round-off error of the CPU (which will be very small) and the resolution of the camera-monitor system (which will also be small).

Another set-up was made and this time, the intersection of the line with the scanning-plane was used in order to prove the validity of the algorithm presented above. A point "S" was located on the laser line scanning an object. The plane of scanning was determined to be:

$$y = 3.606$$

The coordinates of that point on the screen were measured to be:

(52, -33)

The camera-frame was:

h = -x

v = -z

a = y

From the above information, the point under consideration was determined to be on the line:

x = -52*t

y = -41 - 675.294*t

z = 33*t

The intersection of that line with the plane "y = 3.606" is:

x = 3.43 vs 3.606

y = 3.606 vs 3.606

z = -2.178 vs -2.800

Another source of error in the calculation above is the determination of the plane of scanning by direct measurement.

The VALII Program

A VALII program was written to perform the above. The listing of that program follows:

```
u = 52
v = -33
xf = 0
yf = -41
zf = 0
f = 675.2942
asp = 0
bsp = 1
csp = 0
dsp = 3.606
xh = 1
yh = 0
zh = 0
xv = 0
yv = 0
```

```
zv = 1
xa = 0
ya = 1
za = 0
xp = u.xh + v.xv + f.xa + xf
yp = u.yh + v.yv + f.ya + yf
zp = u.zh + v.zv + f.za + zf
temp = asp.xf + bsp.yf + csp.zf
temp1 = asp.xp + bsp.yp + csp.zp
t = (dsp - temp)/(temp1 - temp)
xr = xf + (xp - xf).t
yr = yf + (yp - yf).t
zr = zf + (zp - zf).t
type /B, x, c2
type /B, y, c2
type /B, z, c2
```

Future Work

Future work should:

1. Identify and implement a way to detect a laser beam on the screen (using the vision processor).

2. Identify and implement a way to detect a broken line (i.e. equations of the straight lines constituting a broken line).

3. Further research towards the identification and handling of non-rigid 3-D objects.

II. Locating Surfaces Using a Range Finder

The program (listing given in III) analyzes an image provided by a camera. It will search for bright lines in the image and determine the equations and boundaries of those lines. From those boundaries, the boundaries of the laser lines that are projected on the object are calculated in 3-D coordinates. Thus the equations of those lines are calculated and the surfaces on which they are projected are determined.

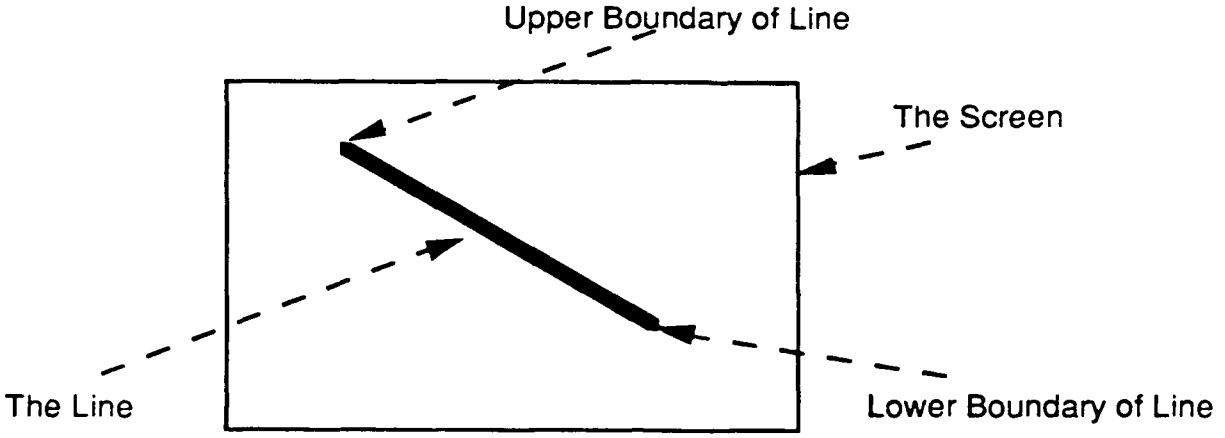

Boundaries of the Image of a Laser-Line

The program begins by assuming that there is a continuous (vertical) laser-line from the top to the bottom of the screen. It tries to locate the boundaries of that line. Beginning with the top, it searches for a bright point. If that point is found, its 2-D position is saved; otherwise, the search is restarted at the next level down the screen. Once the upper boundary of the line is located, the same procedure is used to locate the lower boundary (i.e. search for a bright point in the bottom of the screen, if not found then move to the next level up). Once the two boundaries are found, the equation of the assumed line is calculated. The program then tries to locate a bright point midway between the two levels.

If a bright point is located, then its coordinates are checked whether they are on the assumed line (or near it by some margin of error). If this is the case, then we have enough reason to believe our earlier assumption. If the point is not on or near the line, then the program assumes that there are two distinct straight-lines and thus updates its list of lines to reflect the presence of both lines (instead of the original line). Then the procedure is started all over for each line in the list.

If two bright points were located (the program does not

detect more than two points), the program assumes that there are two distinct straight-lines, the two points just detected correspond to the boundaries of those lines (the beginning of the lower line and the end of the higher one). The list of lines to be checked is updated accordingly and the procedure is repeated for each line in the list.

If no bright point has been detected, then there are two straight-lines, the upper boundary of one and the lower boundary of the other are not known. The program locates those boundaries using a modification of the procedure that located the boundaries of the initially assumed line. After locating those boundaries, the list of lines to be checked is updated and the procedure is repeated for each line on the list.

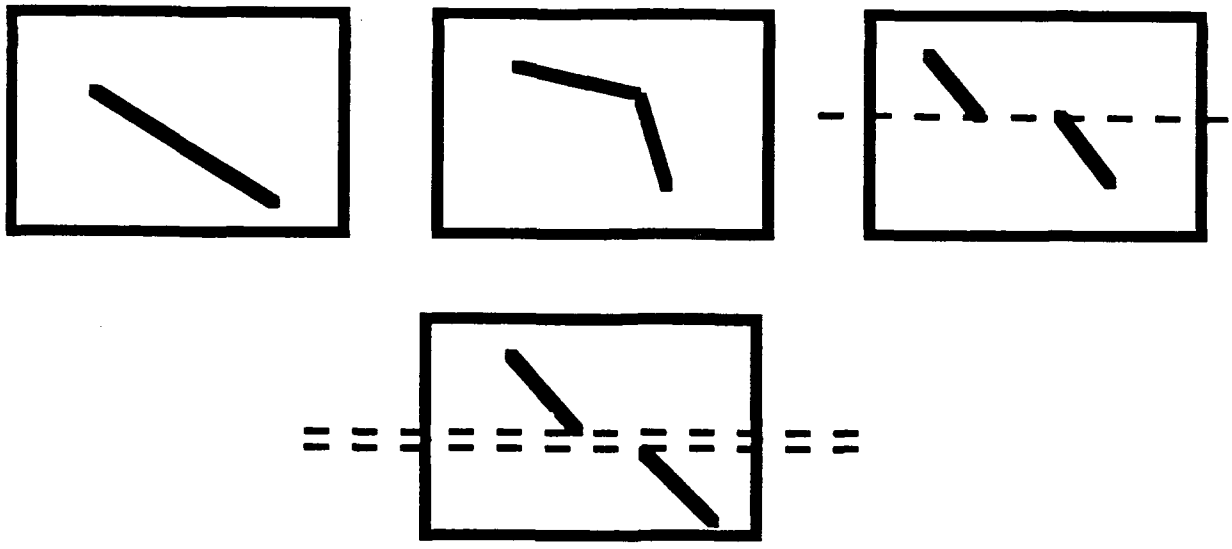

Possible Patterns of Lines to be Detected

Once the boundaries of a straight-line and its existence are established, the program returns its boundaries and moves to check the next line on the list. This is done until all candidate lines are checked.

The output of this program can be used by our earlier program to get the boundaries of the laser-lines in 3-D coordinates. Knowing those boundaries, we can derive the information we need about the object (e.g. depth of the object is the distance between the two shifted lines).

This program still needs some refinements:

1. Experiment with different objects to check the validity of the algorithm described above.

2. Currently, the program approximates curves by a series of two-point lines. This matter must be studied further to determine the best way to identify curves.

3. Many assumptions were made throughout the writing of this algorithm. These assumptions are valid for the objects that were under study (a cube and planar surfaces), the validity of those assumptions must be determined for a larger number of objects (and if possible investigate the theory behind them).

4. The program assumes ideal lines in the image (i.e. width of the laser-line is 1 pixel on the screen), a way to identify lines with varying width should be investigated. This should be done by experimenting with different objects to identify the maximum width of a laser line and how it varies with the type of material of the scanned surface.

5. A method to speed up the search for lines should be investigated if the current method does not meet our real-time constraints.

Future research should also concentrate on object recognition. A method should be found to recognize rigid as well as non-rigid objects. The vision and range-finder information integration must be studied as well. Also another area of study towards the recognition of non-rigid objects, is the database of objects that should be built and the Artificial Intelligence aspect behind the recognition process.

III. The Listing of the Program

The program consists of a main routine (LASER.LINE) and supporting subroutines.

The listings of all routines follow:

LASER.LINE

```
        Call v.init
        Threshold = 200
        Call v.erase.graphics
        Call v.scan
        Call v.freeze
        Call get.first
        If level[1] == 255 goto 200
        k = 0
        plist = 10
        nlines = 1
        xbpoint[plist] = u[1]
        ybpoint[plist] = v[1]
        xepoint[plist] = u[2]
        yepoint[plist] = v[2]
        Call LOCATE.LINE
200     Type /B,"No More Lines"
```

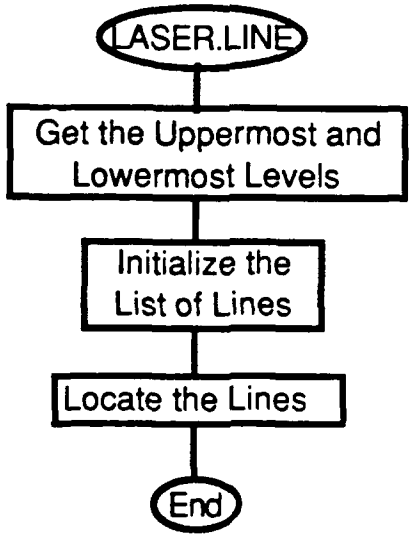

```
GET.FIRST

          level[1] = 0
          level[2] = 255
        1 j =1
          lev = level[1]
          Call DETECT.LIGHT
          if (v.reply[1] < Threshold and level[1] < 255) then
                    level[1] = level[1] + 1
                    Call v.erase.graphics
                    Goto 1
          End
          if level[1] == 255 then goto 100
          Call GET.POINT
        2 j =2
          lev = level[2]
          Call DETECT.LIGHT
          if (v.reply[1] < Threshold) then
                    level[2] = level[2] - 1
                    Call v.erase.graphics
                    Goto 2
          End
          Call GET.POINT
      100 Return
```

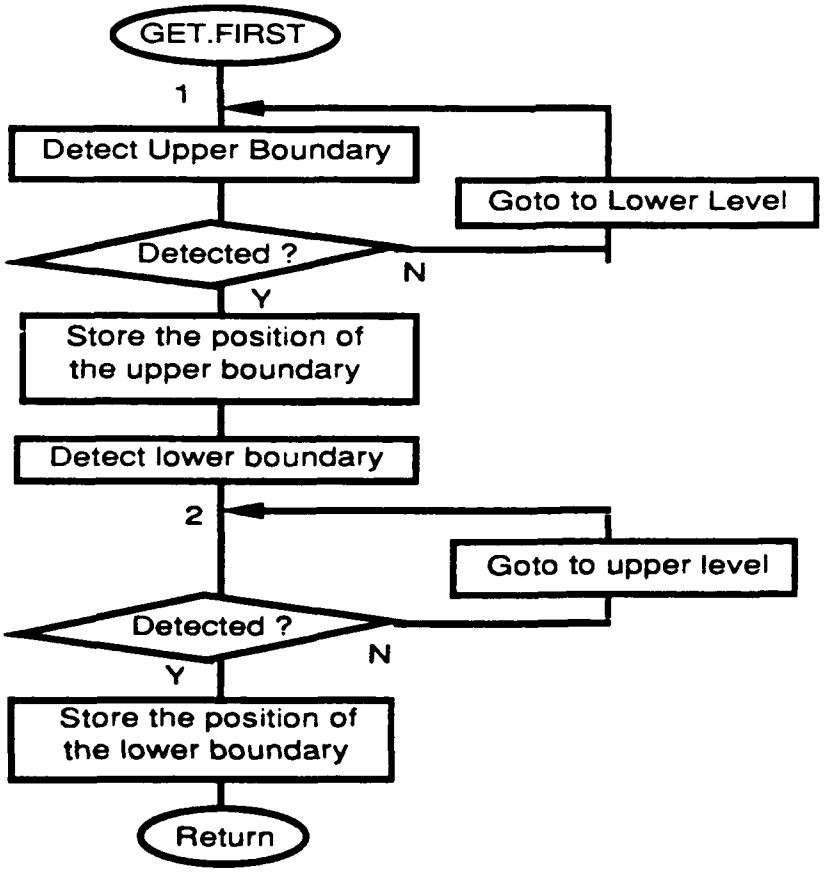

```
LOCATE.LINE
        3 u[1] = xbpoint[plist]
          v[1] = ybpoint[plist]
          u[2] = xepoint[plist]
          v[2] = yepoint[plist]
          Call BRROKEN.OR.NOT
          if shift then
               xepoint[plist + 1] = xepoint[plist]
               yepoint[plist + 1] = yepoint[plist]
               xbpoint[plist + 1] = u[4]
               ybpoint[plist + 1] = v[4]
               xepoint[plist] = u[3]
               yepoint[plist] = v[3]
               nlines = nlines + 1
          End
          If connected then
               if broken then
                    xepoint[plist + 1] = xepoint[plist]
                    yepoint[plist + 1] = yepoint[plist]
                    xbpoint[plist + 1] = u[3]
                    ybpoint[plist + 1] = v[3]
                    xepoint[plist] = u[3]
                    yepoint[plist] = v[3]
                    nlines = nlines + 1
                    Goto 3
               End
               xe[k] = xepoint[plist]
               ye[k] = yepoint[plist]
               xb[k] = xbpoint[plist]
               yb[k] = ybpoint[plist]
               plist = plist + 1
               Type /B, "k = ",k
               Type /B, "xb = ",xb[k],/X10,/S
               Type /B, "yb = ",yb[k]
               Type /B, "xe = ",xe[k],/X10,/S
               Type /B, "ye = ",ye[k]
               k = k + 1
               nlines = nlines -1
               if nlines goto 3
               Return
          Else
               Call LOCATE.DISCONNECTION
               nlines = nlines + 1
               Goto 3
          End
```

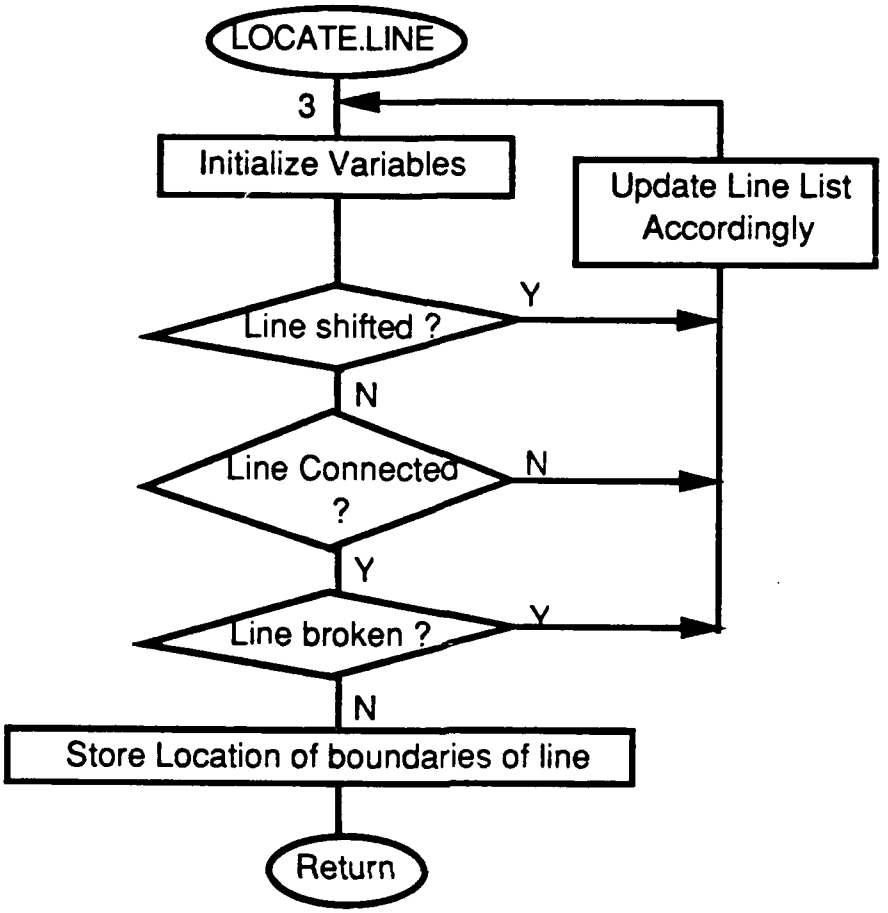
LOCATE.LINE
3
Initialize Variables
Update Line List Accordingly
Line shifted ?
Y
N
Line Connected ?
N
Y
Line broken ?
Y
N
Store Location of boundaries of line
Return

BROKEN.OR.NOT

```
a = (v[1] - v[2])/(u[1] - u[2])
b = v[1] - a*u[1]
level[3] = 128 - (v[2] + v[1])/2
lev = level[3]
Call DETECT.LIGHT
if V.Reply[1] < Threshold then
     connected = 0
                              else
     connected = 1
     Call GET.POINT
     if abs(v[3] - a*u[3] - b) > 2 then
          broken = 1
                                   else
          broken = 0
     End
End
Return
```

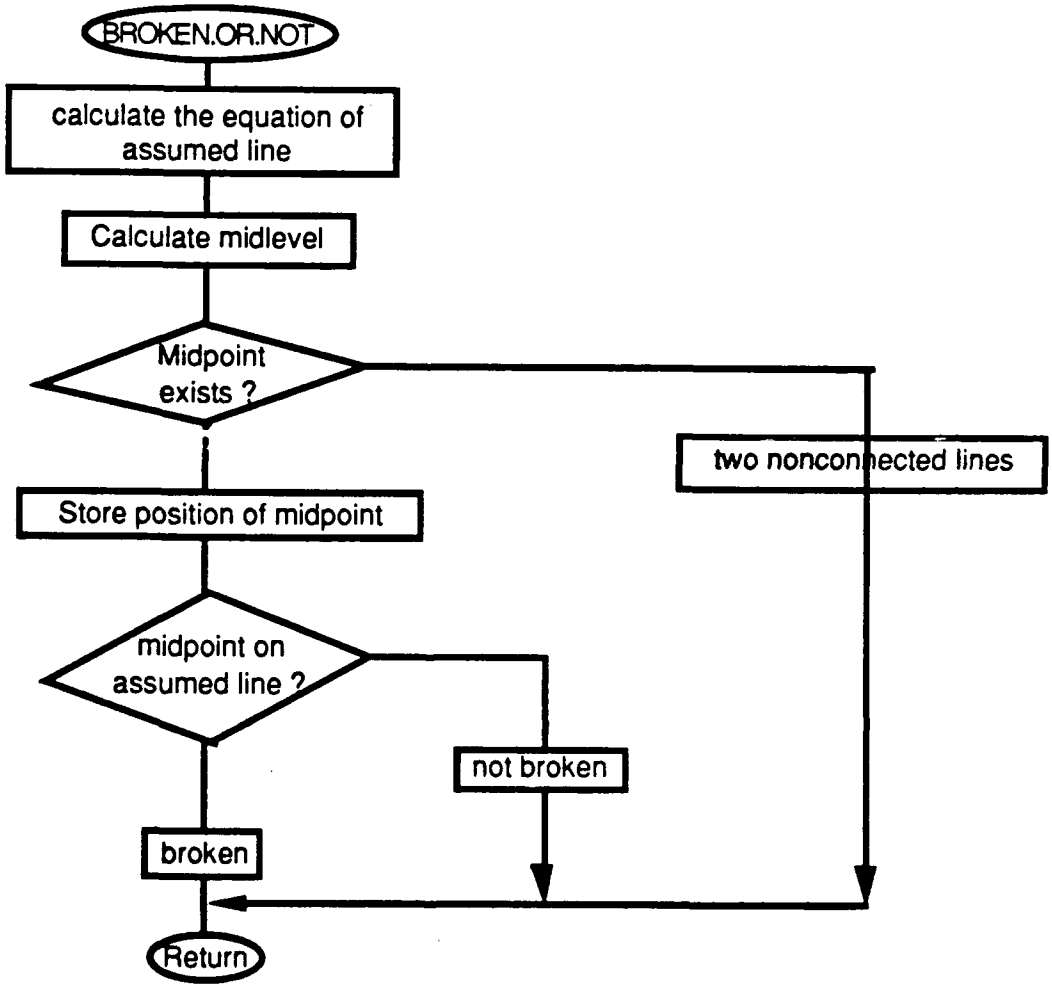

```
DETECT.LIGHT

        v.x = 0
        v.y = lev
        Call v.move.point1
        v.x = 255
        Call v.move.point2
        Call v.draw.line
        v.spacing = 0
        Call v.get.minmax
        Return
```

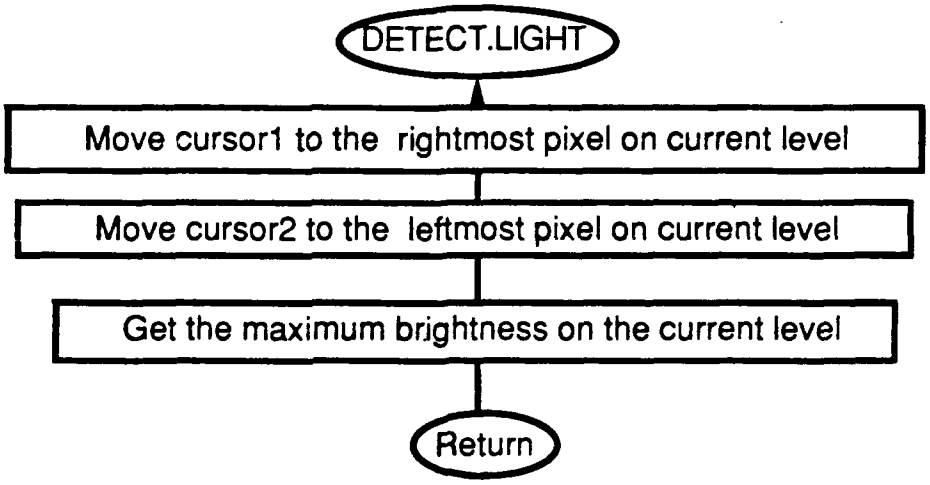

GET.POINT

```
one = 0
Call v.get.graph
For i = 1 to 255
     if v.reply[i] > Threshold then
          if one then j = 4 End
          v[j] = 128 - v.y
          u[j] = i - 128
          one = 1
     End
     if one then shift End
     one = 0
     if u[4] < u[3] then
          temp = v[3]
          v[3] = v[4]
          v[4] = temp
          temp = u[3]
          u[3] = u[4]
          u[4] = temp
     End
End
Return
```

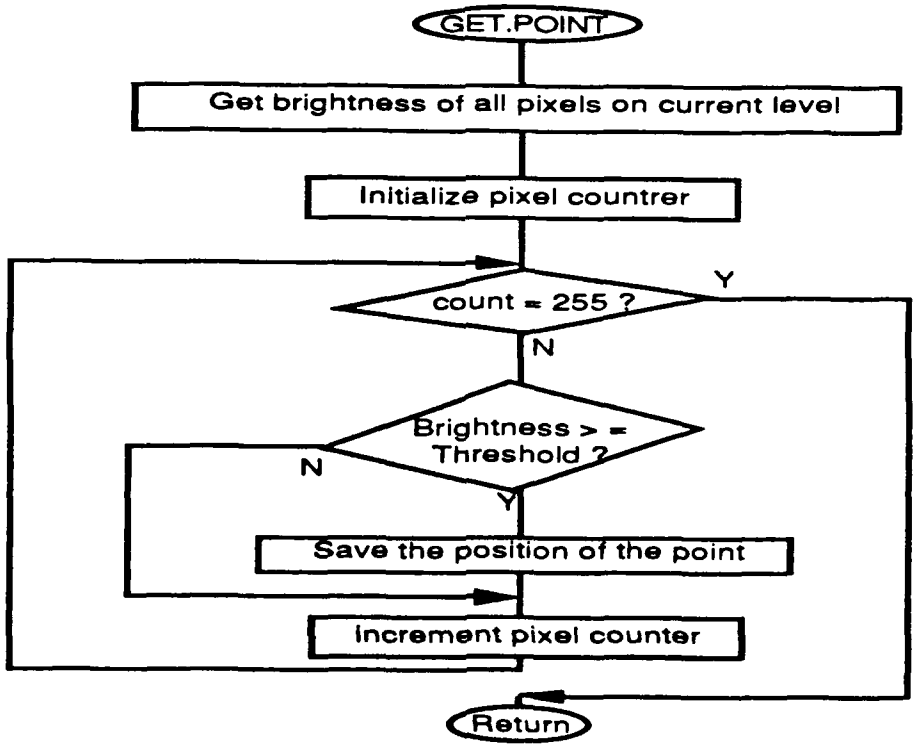

LOCATE.DISCONNECTION

```
      lev = level[3]
4     lev = lev - 1
      Call DETECT.LIGHT
      if V.Reply[1] < Threshold then
           goto 4
                                  else
           j = 3
           Call GET.POINT
           xepoint[plist] = u[3]
           yepoint[plist] = v[3]
      End
      lev = level[3]
5     lev = lev + 1
      Call DETECT.LIGHT
      if V.Reply[1] < Threshold then
           goto 5
                                  else
           j = 3
           Call GET.POINT
           xbpoint[plist] = u[3]
           ybpoint[plist] = v[3]
      End
      Return
```